Commissioning of the self-trigger of the TARGET read-out-board for FAMOUS

von

Benjamin Jan Pestka

Bachelorarbeit in Physik

vorgelegt der
Fakultät für Mathematik, Informatik und Naturwissenschaften
der
Rheinisch Westfälischen Technischen Hochschule Aachen

im September 2016

angefertig am

III. Physikalischen Institut A

Erstgutachter

Prof. Dr. Thomas Bretz
III. Physikalisches Institut A
RWTH Aachen

Zweitgutachter

Prof. Dr. Thomas Hebbeker
III. Physikalisches Institut A
RWTH Aachen

Contents

1. Introduction

Every day, cosmic rays hit the atmosphere and create air showers. The Pierre Auger Observatory is the largest project to detect and analyse these showers. To detect fluorescence light, the Pierre Auger Observatory uses photomultiplier tubes (PMTs). A promising alternative to PMTs are Silicon photomultipliers (SiPMs), which are used in the FAMOUS telescope.
The FAMOUS (**F**irst **A**uger **M**ulti-pixel photon counter camera for the **O**bservation of **U**ltra-high-energy cosmic air **S**howers) project started at the RWTH Aachen. The FAMOUS telescope is a prototype for an air fluorescence telescope based on SiPMs. For the read out of the FAMOUS telescope the TARGET7-module (TeV Array with GSa/s sampling and Experimental Trigger) is used, which was developed for the Cherenkov Telescope Array (CTA).
In this Bachelor-thesis the first steps for the commissioning of the self-trigger of the TARGET7-module will be done. Furthermore, characteristics of the TARGET7-module will be inspected and presented. In the end the results of night measurements outside with the TARGET7-module as the readout board for the FAMOUS telescope will be presented.

1.1 Cosmic rays and the Pierre Auger Observatory

Cosmic rays are fast-moving particles from space that hit the earth and the atmosphere constantly and from all directions [1]. There are two different types of cosmic rays:
The primary cosmic rays, which are those particles which came from astrophysical sources and have high energy up to 10^{20} eV. Mostly, this primary cosmic rays are atomic nuclei [2].
The secondary cosmic ray arises from interaction of the primary cosmic rays with interstellar gases.
If a primary cosmic ray hits the atmosphere, there arises a shower of secondary cosmic particles like it is shown in figure 1.1.

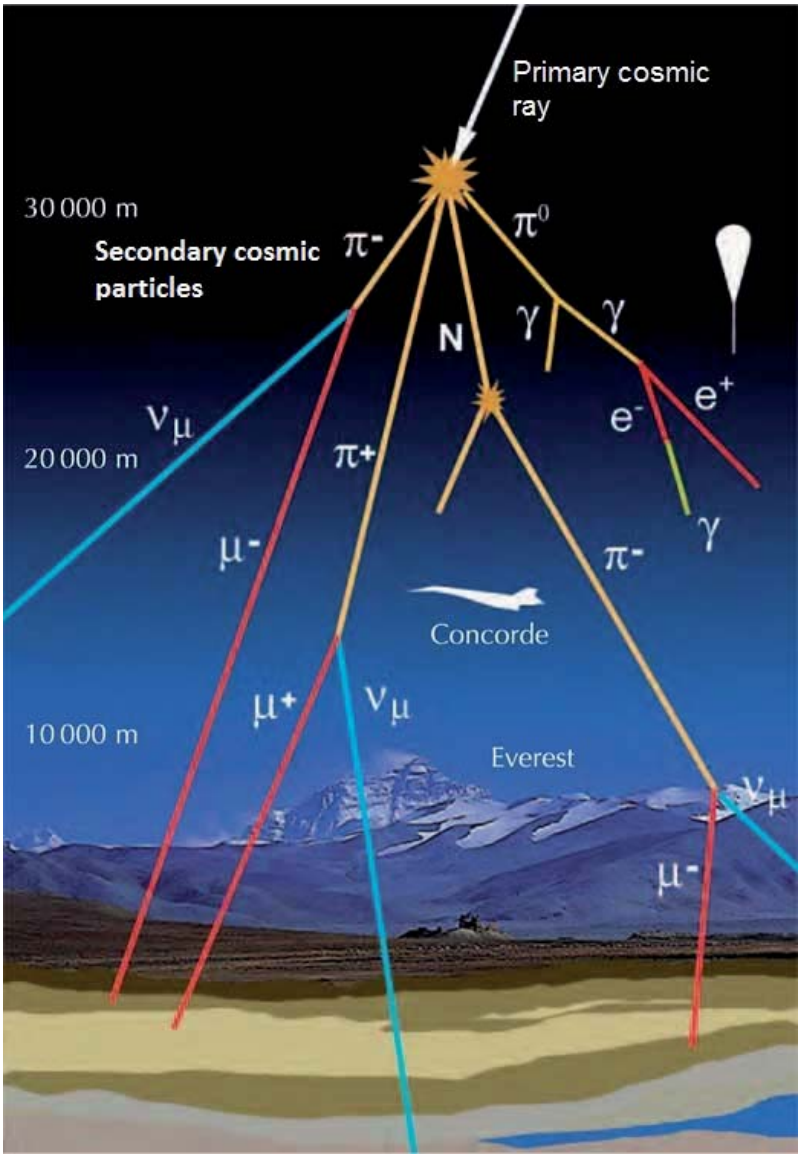

Figure 1.1: In this figure is shown an schematic of an air shower. When the primary cosmic ray hits the atmosphere a lot of other particle arise and move on to the earth. On different hight there can be measured different particles which have been created [3].

Figure 1.2: An air shower at the Pierre Auger Observatory [4]

It is possible to measure the secondary cosmic particles on the earth, because the primary cosmic ray interact with the atmosphere. With the measurement of the secondary particles it is possible to reconstruct the whole air shower so that the energy and the direction of the primary particle can be obtained. The highest-energy cosmic rays have more thant ten million times higher energy than the particles produced in the world's most powerful particle accelerator. Therefore, it is very interesting for particle physiscists [1].
To study this air-showers lot of physicists works together such as at the Pierre Auger Observatory in Argentina. The Pierre Auger Observatory is the largest experiment to investigate the cosmic rays.
To detect the secondary cosmic ray, the Pierre Auger Observatory uses hybrid detectors, employing two independent methods:
One technique detects high energy particles through their interaction with water. Therefore water tanks with surface detectors (SD) in the tanks are used. The Auger Observatory uses 1660 of these water tanks, spread across 3000 km^2 arranged in a grid as seen in figure 1.5 and equipped with three photomultiplier tubes (PMTs) each to detect Cherenkov light. Cherenkov light is created, when a particle moves faster than light in a medium, so that $v > cn^{-1}$ with v as the speed of the paricle, c as the speed of light in the vacuum and n as the refractive index of the medium [5]. The Cherenkov Photons are emitted with the Cherenkov-angle $cos(\Theta_C) = (nc\beta)^{-1}$, with $\beta = vc^{-1}$, as one can see in figure 1.3. In the Pierre Auger Observatory the Cherenkov light is created in the water tanks and than detected by the PMTs [6].

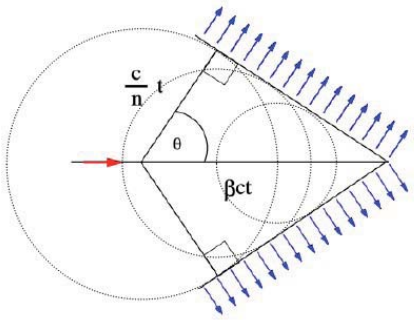

Figure 1.3: The figure shows in which angle to the particle the Cherenkov-shower is emitted when the particle moves faster then light in a medium [5].

The second technique tracks the development of air showers by observing ultraviolet fluorescence light emitted high in the Earth's atmosphere. The spectrum of the emitted fluorescence light is mostly in the ultraviolet area as it can be seen in figure 1.4b. To detect the fluorescence light the Pierre Auger Observatory the fluorescence detector (FD) which contains 27 fluorescence telescopes, located at five different stations overlooking the SD tanks (figure 1.5). The design of the telescope is based on Schmidt optics [6] and can be seen in figure 1.4a. Via the segmented mirror, the fluorescence light is reflected to the pixel camera containing 440 photomultipliers arranged in a matrix of 22 rows by 20 columns each with a field of view of 1.5° x 1.5° [6]. The shower axis and spread can be reconstructed, so that the energy and arrival direction of the cosmic particle can be obtained [6].

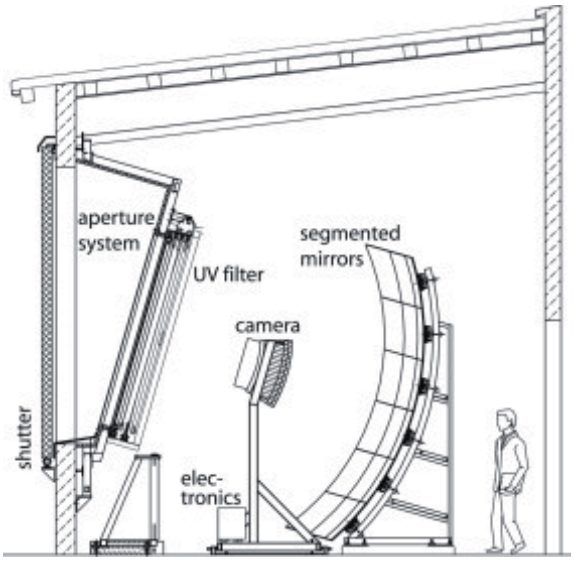

(a)

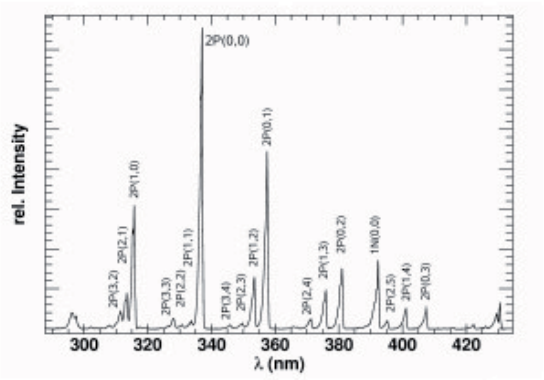

(b)

Figure 1.4: Left: Schematic view of a fluorescence telescope with a description of its main components [6].
Right: The spectrum, intensity vs. wavelength, of fluorescence light. The intensity between 300 nm and 400 nm is mostly created by de-exciting Nitrogen in the atmosphere after being excited by secondary particles in the extended air shower [7].

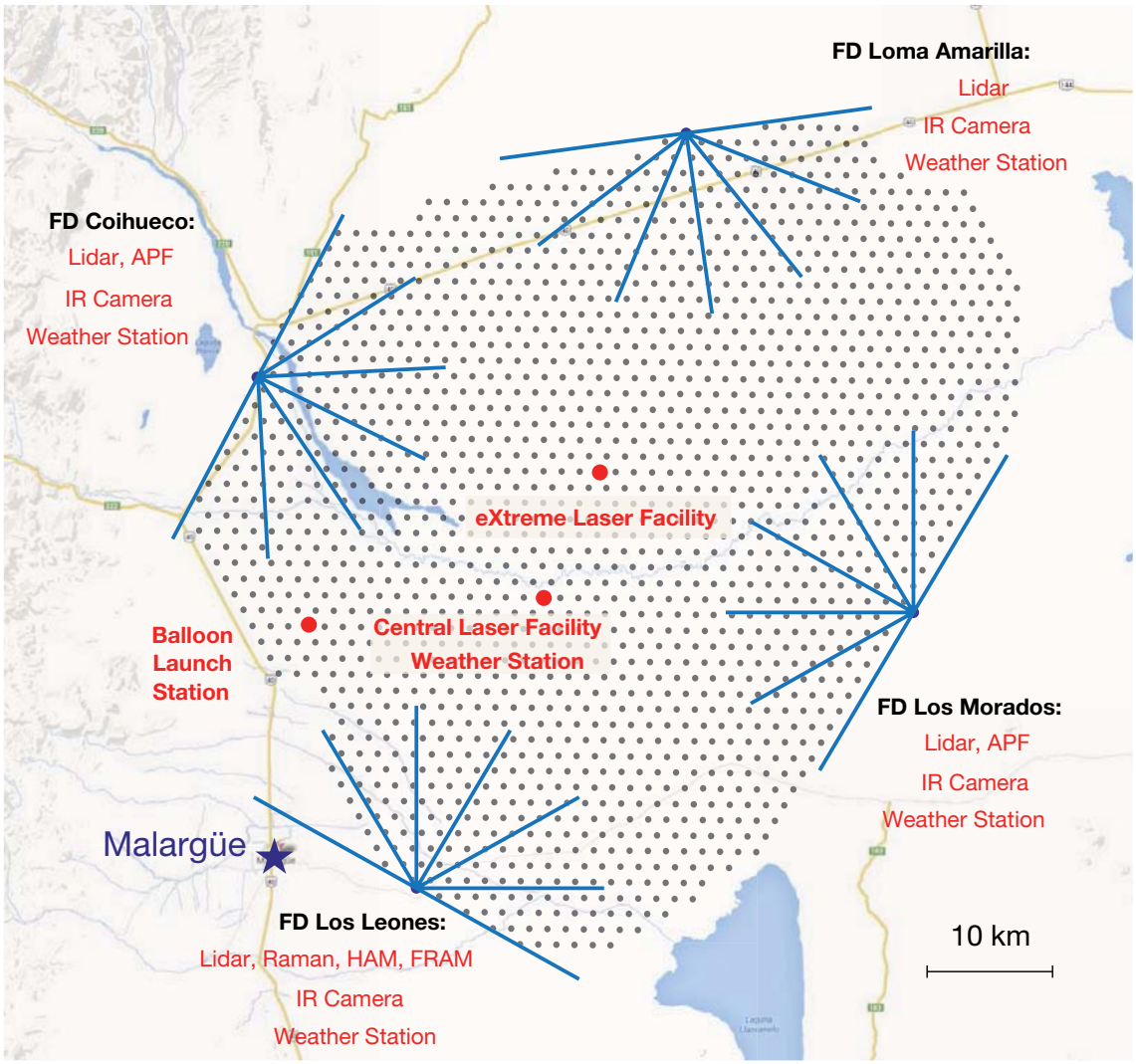

Figure 1.5: Map of the Pierre Auger Observatory. Each dot represents a surface detector (SD) tank, the lines represents the limits of the flouressence detectors field of view [8].

1.2 FAMOUS

FAMOUS (**F**irst **A**uger **M**ulti-pixel photon counter camera for the **O**bservation of **U**ltra-high-energy cosmic air **S**howers) is a small fluorescence telescope (Figure 1.6b), based on silicon photomultipliers (SiPMs) for optical read-out, developed at III. Physikalisches Institut A, RWTH Aachen University [9].
The FAMOUS telescope consists of a Fresnel lens with a diameter of $D = 510\,\text{mm}$ equal to the focus length. With the lens the light is focused to 61 Winston cones which directs the photons to the SiPMs. The Winston cones are arranged in a hexagonal structure like it is shown in figure 1.6a. Each of this SiPMs has a view of 1.5° x 1.5°. There are three more SiPM pixel in the telescope which are "blind", so that they can not be hit by any photons. They are useful for measure the electronic noise and the SiPM noise during the actual measurement.

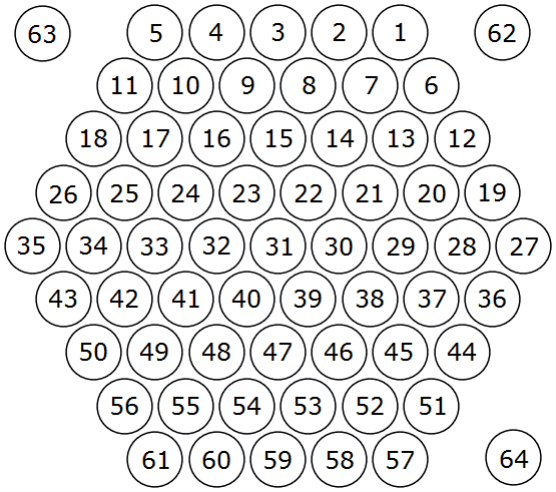

(a)

(b)

Figure 1.6: Left: The hexagonal structure of the 61 pixel in the FAMOUS telescope and the three blind pixel at the side.
Right: The FAMOUS-telescope in the hall of physics at the center of physics, RWTH Aachen, Germany. Picture made by Benjamin Pestka.

2. Silicon Photomultipliers

In this chapter the silicon photomultipliers (SiPM) will be presented, how they work and which characteristics they have. Advantages and disadvantages of SiPMs will be discussed.

Photodiode

Silicon is a semiconductor which makes it possible it is possible to count single photons. At first it will be explained how a semiconductor works:
A semiconductor has a valence band and a conduction band. For $T \to 0\,\mathrm{K}$ all electrons are in the valence band. When the temperature increases, the thermal energy of the electrons increases too. When $E_{thermal} > E_\mathrm{G}$, the electrons can pass the band gap and get to the conduction band (figure 2.1a). When an electron gets to the conduction band, it leaves a hole in the valence band which can be seen as an positive charge in the valence band. When applying a voltage U_bias, the electrons in the conduction band move free to the positively charged anode while the holes in the valence band move to the negatively charged cathode. Both mechanisms increase the current [10].
If an electron gets to the conduction band due to thermal excitation or the absorption of a photon, the voltage changes a bit and this change can be measured. If the thermal noise is small because of a low temperature like $T = 10\,\mathrm{K}$, single photons can be measured [10].
It is possible to dope semiconductors. This means that there are implanted another sort of atoms, mostly from the III or V main group of the period table, which brings new energy levels to the band structure. The new energy levels are between the valence band and the conduction band. Doping the semiconductor can be done in two different ways:
A n-doped semiconductor gets a new energy level near the conduction band, by adding pentavalent atoms. The electrons from the donor do not have to have the energy E_G to pass the band gap and pass to the conduction band, instead they need a smaller energy (figure 2.1b). The electrons can move freely in the conduction band and it does not matter if they are from the valence band or the donor.

A p-doped semiconductor gets a new energy level near the valence band, by adding trivalent atoms. This energy level can be used as an acceptor (figure 2.1c) so that the electrons from the valence can use this it as a conduction band. The energy difference between the valence band and the acceptor band is much smaller than E_G so that less energy is required for a current to flow.
It is also possible to get an p-n-doped semiconductor with both energy levels between the valence band and the conductor band [10]. This means that the electrons have more possibilities to absorb photons to change the energy level, so that they can contribute to the current flow.

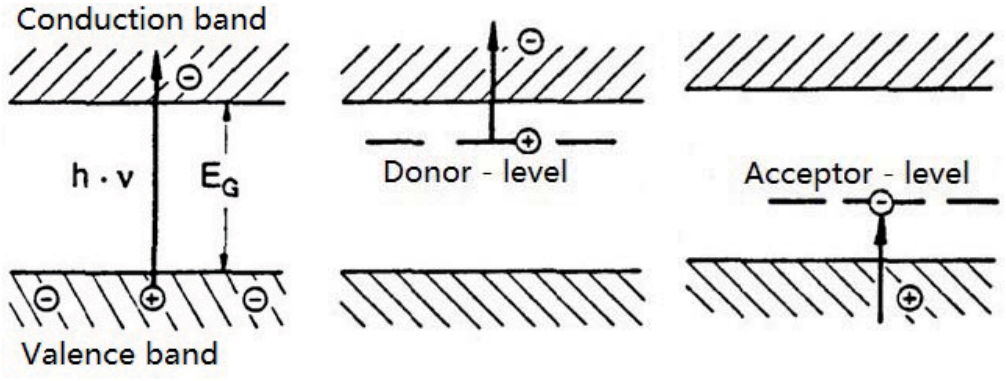

(a) (b) (c)

Figure 2.1: Left figure: direct band absorption; middle figure: Transition from donator to conduction band by absorption of a photon; right figure:Transition from valence band to acceptor by absorption of a photon.
All figure taken from [10] and edit by Benjamin Pestka.

Avalanche Photodiode (APD)

With an avalanche photodiode (APD) a higher output voltage and higher output current can be reached than with an intern amplification mechanisms. An APD excited with a great reverse voltage so that charge carriers, by a photon absorption, are sloped in the electric field E. If the charge carriers are accelerated, they can reach enough energy to free other charge carriers by collision with lattice atoms (figure 2.2a) [10].
If the holes would be accelerated in the same way as the electrons, they could cause electron avalanches too. This would be a big noise factor so that the amplification of the holes has to be decelerated. This can be done by a coating structure with a variable band gap built like a saw tooth form in direction of the field lines as seen in figure 2.2b. When the holes try to accelerate, they have to overcome the growing growing potential. The growing potential causes a deceleration of the holes so that the amplification is reduced by a factor of 50-100 [10].
Advantages of the APDs in relation to the traditional photomultiplier are:
A lower power supply is needed and a greater quantum efficiency of 70 % can reached.
A disadvantage of the APDs in relation to the traditional photomultiplier is the smaller sensitive surface. If there is an extended fluorescence light source, the traditional photomultiplier would detect more photons. Futhermore, the amplification is smaller [10].

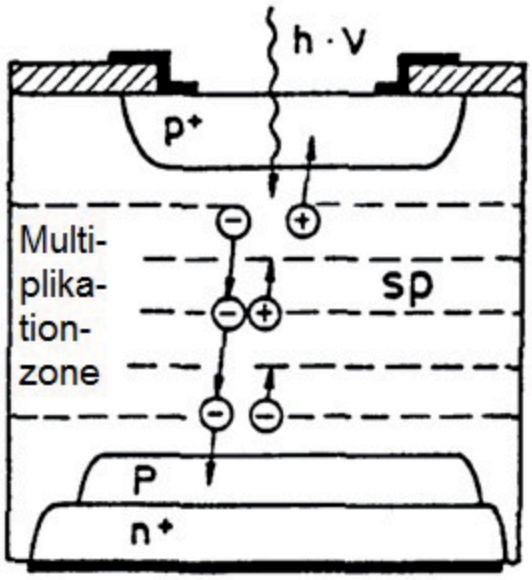

(a)

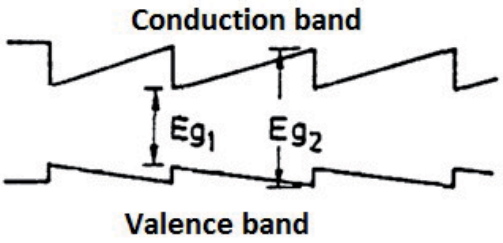

(b)

Figure 2.2: Left: An electron absorbs a photon and gets enough energy to leave the band. At the same time a hole arises. The electron accelerates and hits other electrons which can leave the band, too. The electrons are accelerated again and they cause an avalanche. The holes are decelerated by the band-structure, so that they do not cause the next avalanche.
Right: located band-structure without an outer electric field. The holes have to work against a growing potential energy if they want to move (holes go to the right side). This band-structure decelerates the holes [10].

Geiger-mode Avalanche Photodiode

The Geiger-mode, named after Hans Geiger and Walther Müller, is an operating mode of a detector and allows the detection of ionizing particles. This means, when the APD operates in Geiger-Mode, it can only detect and count the photons, but it can not determine the energy of them.
When the APD receives a bias voltage above the breakdown voltage V_{bd} the electrons and holes multiply by impact ionization faster, on average, that they can be extracted. The breakdown voltage V_{bd} is the minimal voltage with which the minimal energy is given to start an avalanche process [11]. It is known that the breakdown voltage increases linear with temperature T:

$$V_{\mathrm{bd}}(T) = V_{\mathrm{bd}}(T_0) + \beta \cdot (T - T_0) \tag{2.1}$$

with $T_0 \equiv T(0\,^{\circ}\mathrm{C})$ and $\beta = const.$ depending on the G-APD-type [12].
The over voltage is known as $V_{ov} = V_{\mathrm{bias}} - V_{\mathrm{bd}}$ and is a measure for the amplification of the signal.
Avalanche photodiodes can detect only one photon at the same time. This can be expended by connecting several APDs in parallel.

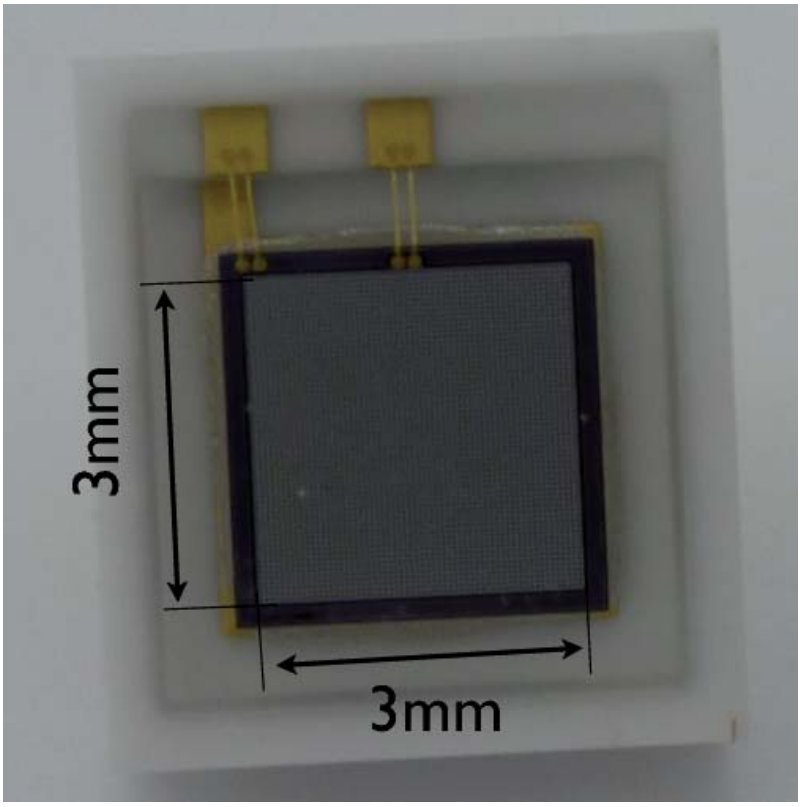

Figure 2.3: Photo of a Hamamatsu S12652-A0013 Silicon Photomultiplier (SiPM)[13].

Silicon Photomultiplier (SiPM)

Silicon photomultipliers (SiPMs) are semiconductor photo detectors which are built-up of hundreds to several tenthousands of small avalanche photodiodes, referred to as cells, operating in Geiger-mode (figure 2.3) [14]. Each cell is able to detect single photons and the dynamic range of the whole device is defined by the number of cells situated on the SiPM. The cell pitch typically lies between 25 μm and 100 μm and is an important property of the SiPMs. A larger cell pitch means less space between the cells and causes a greater sensitive surface. Otherwise, a larger cell pitch is correlated with a limited dynamic range.
The cells are connected in parallel like it is shown in figure 2.4.
Due to the connection of the cells, noise is correlated. The different noise phenomena will be discussed:
An avalanche breakdown can be caused by thermal charge carriers and it does not have to be caused by an photon. If it was thermal noise or a signal made by a photon, the signal can not be differentiated. Because of the thermal noise SiPM signals are also observed in dark measurements. The typical noise rate at room temperature for dark measurements is $f_{\mathrm{th}} = 1\,\mathrm{MHz}$ [14]. The dark noise is not only caused by thermal charge carriers. There are also two different kinds of correlated noises: optical crosstalk and afterpulsing.

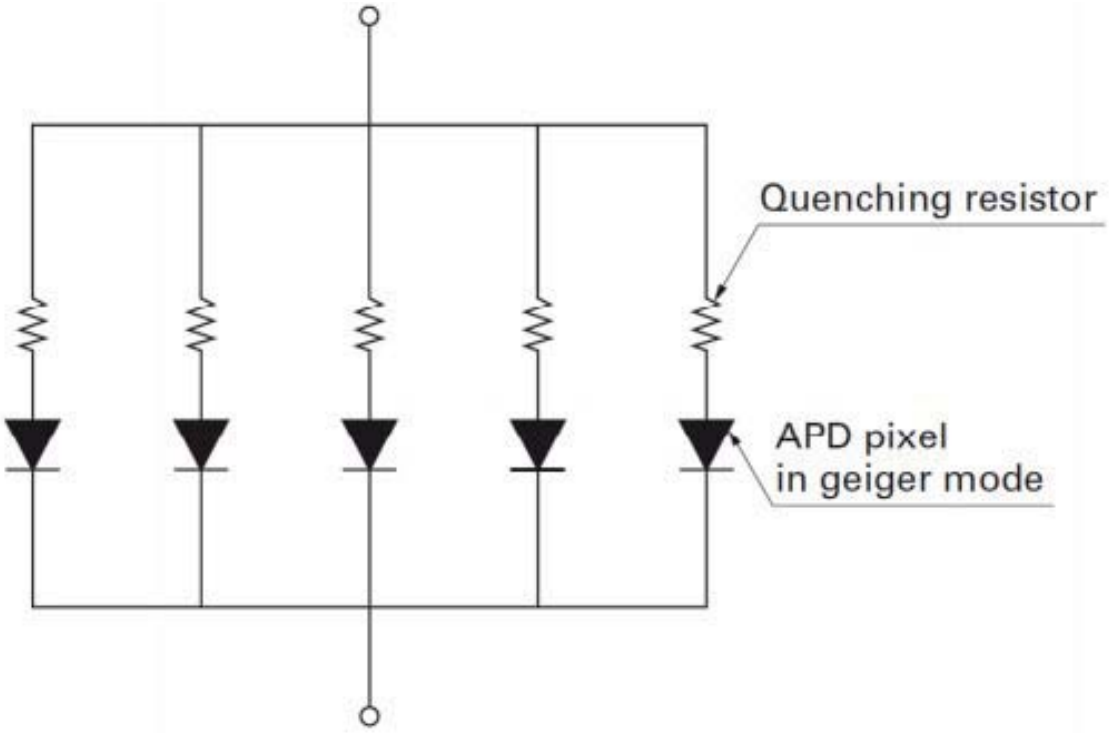

Figure 2.4: Electrical diagram of a SiPM. Each diode represents a G-APD, connected in parallel [15].

Optical Crosstalk
If an avalanche is caused by thermal charge carriers or because of the absorption of a photon, the charge carriers of the avalanche can emit photons too. This photon can cause a cell breakdown in a neighbour cell. This noise phenomenon is called "optical crosstalk"or shortly "crosstalk"[14].
Afterpulsing
The second correlated noise phenomenon is called "afterpulsing ". During an avalanche some charge carriers can be trapped at impurities of the silicon of the SiPM. After a characteristic time τ the charge carriers can be released again and cause a new breakdown avalanche in the cell. The time τ is usually the time needed to replenish the avalanche zone of the SiPM cell [14].
The dark noise is very useful for the measurement of the "gain"of the SiPMs. The gain of a SiPM is the value of the charge which is sent out when exactly one cell absorbed a photon which caused an avalanche. All cells should have the same gain. With the measurement of the voltage of the SiPM and the known resistance of the oscilloscope the current can be calculated. The charge can be calculated by integration of the current over the time. It is possible to determine the number of photons, which hit the detector by the knowledge of the gain and the signal. A SiPM signal during a dark measurement can be seen in figure 2.5.
After calculation of the charges of all the pulses in a dark measurement by integration of the current over the time, the values can be shown in a histogram. The gain of the SiPM is equal to the distance between the peaks, or "fingers" , in the histogram. An example is shown in figure 2.6:

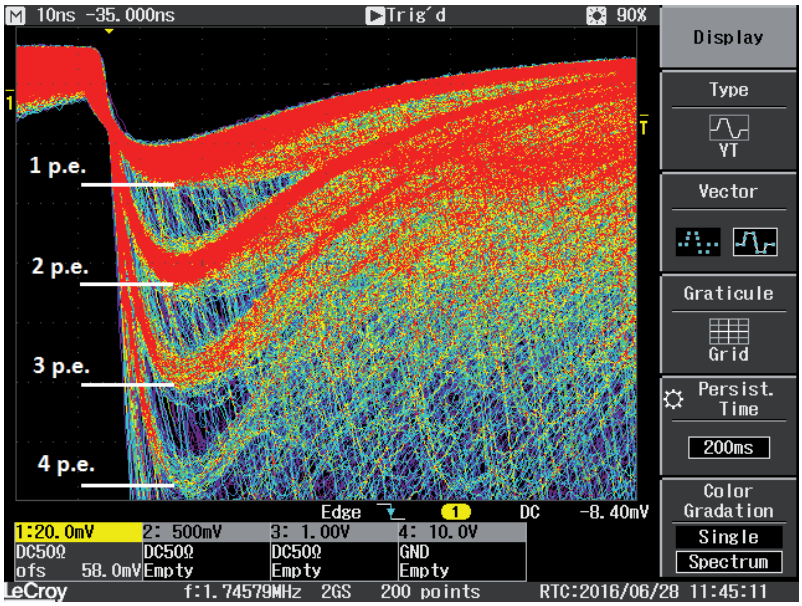

Figure 2.5: Screenshot with an oscilloscope of an amplified signal of a silicon photomultiplier in the FAMOUS type telescope during a dark measurement. The first negative peak is called the one photon electron (p.e.) peak, the second peak the two p.e. peak and so on Markers for the p.e. peaks are added. The screenshot is printed via LeCroy WJ354A at 50 Ω loaded. The horizontal axis represents the time (1 div $\widehat{=}$ 10 ns), the vertical axis represents the voltage (1 div $\widehat{=}$ 20 mV). The event rate is color coded.)

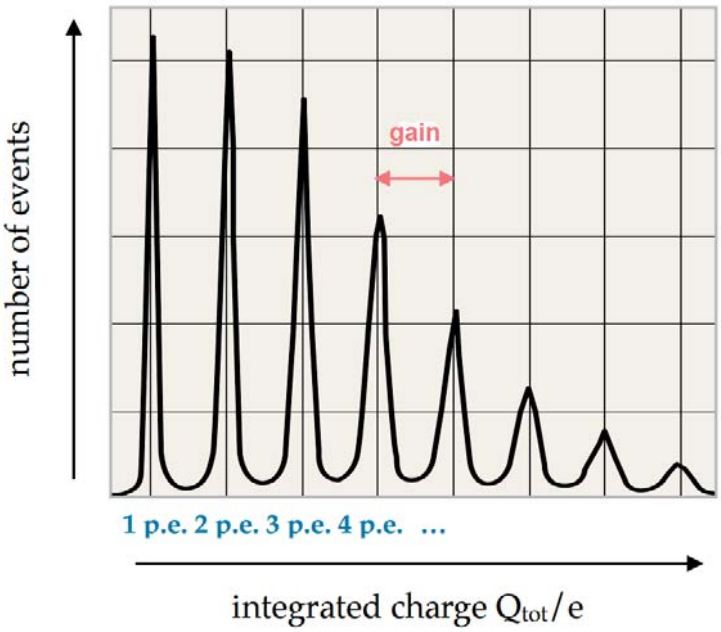

Figure 2.6: Sketch of a histogram of the integrated charge of a SiPM pulse to determine the gain of the cell[16].

SiPMs in the FAMOUS Telescope

In the FAMOUS-telescope the Hamamatsu S10985-100C array of four 3 x 3 mm^2 SiPMs is used [17]. Figure 2.7 shows a technical drawing of the SiPMs, used in the FAMOUS telescope. As it is seen in figure 2.7, the effective active area of the pixel

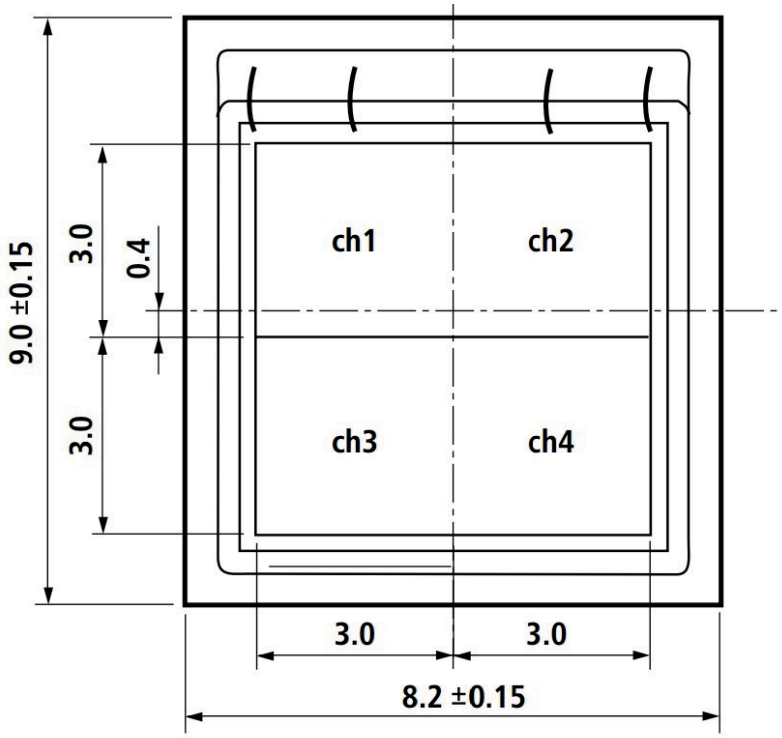

Figure 2.7: Technical drawing of a SiPM in the FAMOUS telescope [18]. All values are given in mm. The sensitive surface is limited at the four channels, where the photons can be detected.

is 6 x 6 mm^2, this is 3 x 3 mm^2 per channel. Each channel includes 900 cells with a cell pitch of 100 μm. 78.5 % of the pixel is a sensitive area and contributes to the detection of photons. The peak sensitive wavelength is 440 nm [18] and is near the wavelength of Cherenkov light (ultraviolet).
The SiPMs are connected to two boards. The QDC (Charge to-digital converter) supplies the SiPMs with the voltage, measures the temperature, regulates the voltage corresponding to the temperature and corresponds with the computer with a LAN-connection for setting the overvoltage. The second board, which is connected to the SiPMs is a adaptor board on which the SiPM-signals are transmitted. At this moment are 20 of the 64 ports at the adaptor-board prepared with cables for transmitting the signals how it can be seen in figure 2.8. There are taken 20 pixels which are in the middle of the camera which are prepared for transmitting the signal, how it can be seen in figure 2.9. 19 of the 20 cables are prepared and connected by Nina Höflich and Benjamin Pestka. In order to ensure that all cables are connected well, test measurements for all cables have been conducted.

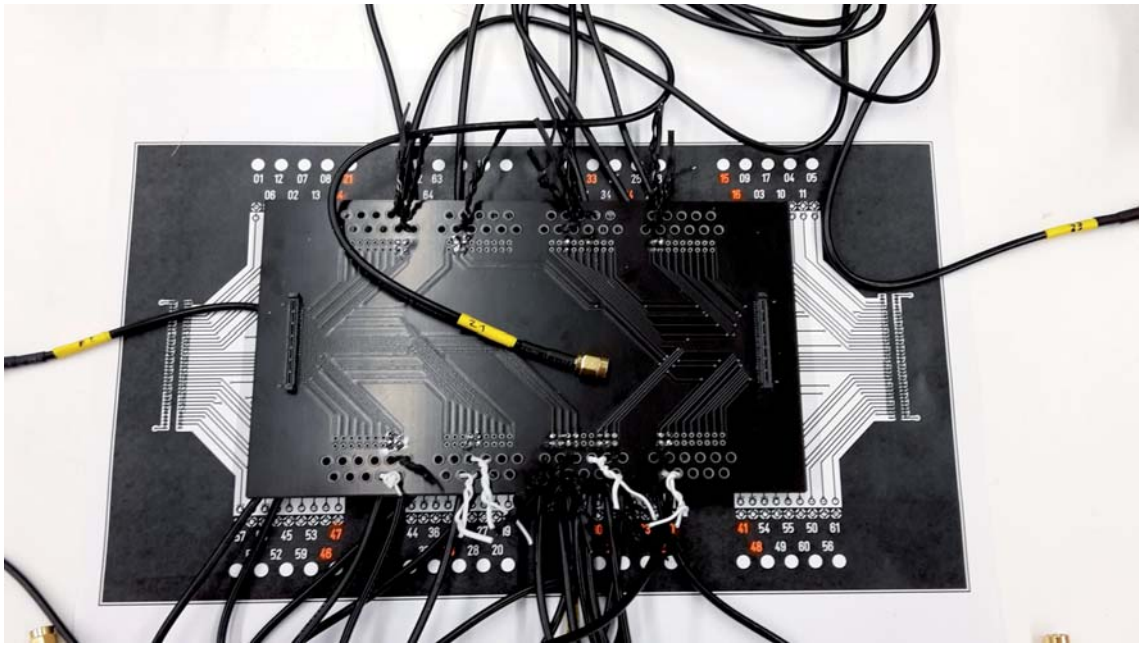

Figure 2.8: Cables prepared and connected to the adaptor-board which can be connected to the SiPMs in the FAMOUS telescope, to transmit the signals. The cables can be connected to the patch board of the TARGET7-module for a readout of the SiPM-signals.

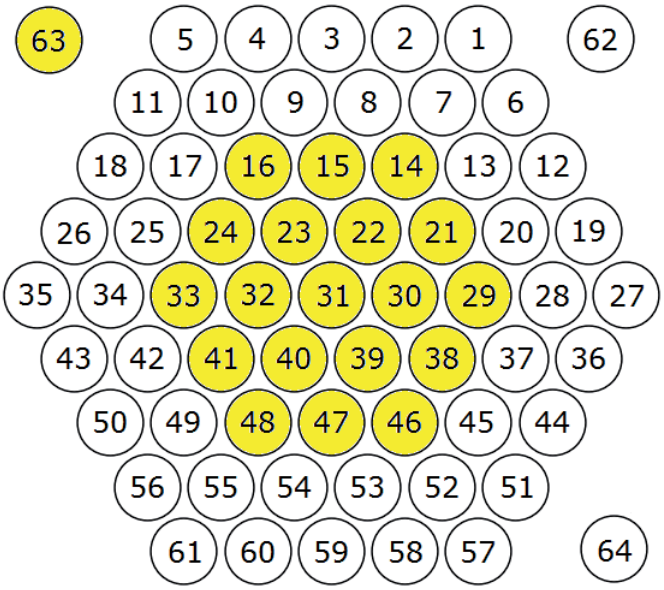

Figure 2.9: The hexagonal structure of the pixels in the FAMOUS telescope. The yellow ones are the pixels which are prepared with cables and ready for read out. To compare the sketch with the real camera, there is a picture of the 64 pixels in figure 5.1 in the appendix. Figure made by N. Höflich [19].

It is very important for the readout that signals can be assigned to the cells. For that reason the cables were marked with a number. To assure that the affiliation is written correctly, they were tested with a weak laser-pointer. Therefore the cable of the pixel is connected to the oscilloscope. If there is only dark noise the measurement looks like it is shown in figure 2.10a. If the laser-pointer is focused at a neighbour pixel of the connected SiPM, the amplitude of the noise reduces. The voltage is nearly constant (figure 2.10b). An explanation for the form of the signal could be, that the cells are hit by photons during the recovery time. This would cause a DC voltage-signal. When the laser-pointer is focused at the SiPM (see figure 5.1 in the appendix), the pixel reaches a constant saturation point and the amplitude of the signal goes down like it is seen in figure 2.10c. This happens because the controlling system disconnect the power supply when the current goes to high.
This method is not advisable to test the right connection of PMTs because they can not handle this much light intensity and they broke. This is another advantage of SiPMs over traditionally PMTs.

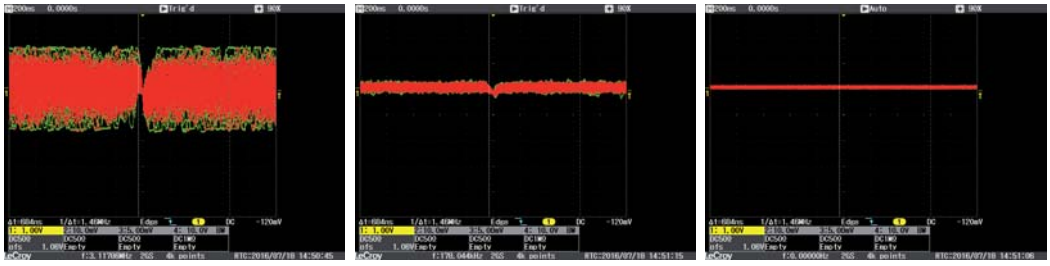

(a) (b) (c)

Figure 2.10: Three sceenshots taken with the oscilloscope. The scale is at each screenshot the same. The x-axis represents the time (1 box$\widehat{=}$200 ns), the y-axis represents the measured voltage (1 box$\widehat{=}$1 V).
Left figure: SiPM trace of a dark measurement of a pixel in the FAMOUS telescope.
Middle figure: SiPM trace of a pixel in the FAMOUS telescope, while a laser-pointer is focused at a neighbour pixel.
Right figure: SiPM trace of a pixel in the FAMOUS telescope, while the laser pointer is focused at this pixel.

3. TARGET 7

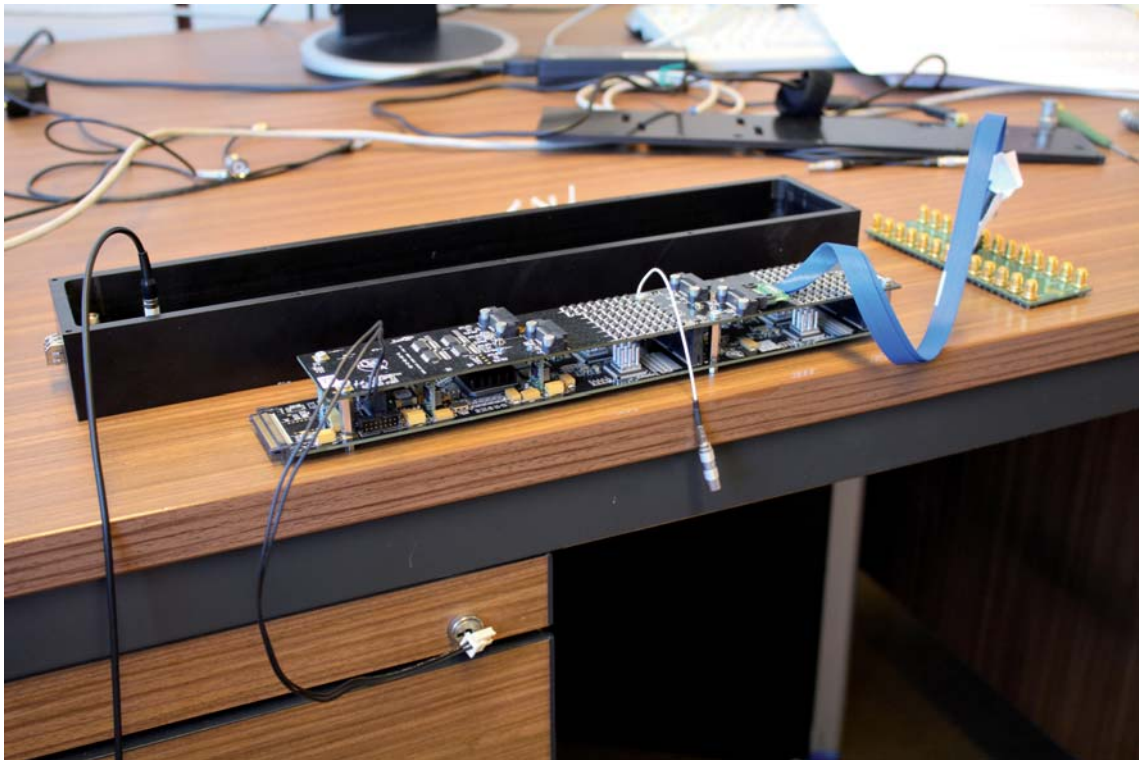

Figure 3.1: The TARGET7-module connected with a ribbon cable to a patch board (green). SMA cables can be connected to it. The TARGET7 board consists of two boards, one above the other. All components are soldered to the boards. The box, in which usually the TARGET7-module is placed, (black box on the figure) is produced in the workshop of institute III. B, RWTH Aachen.

TARGET, TeV Array with GSa/s sampling and Experimental Trigger, module can take data with a sampling rate of one GSa/s. The TARGET7-module offers the opportunity to read out 64 channels with three different trigger types (see chapter 3.3) so that the TARGET7 is an economic and compact module to read out of the 64 pixels of the FAMOUS telescope [20].

Origionally, the TARGET7 is produced for the CTA-Observatory (Cherenkoc Telescope Array) to read out the photo-detectors in telescopes. The CTA-Observatory is an observatory for ground-based gamma-ray astronomy. It is a project with the initiative to build the next generation ground-based very high energy gamma-ray instruments.[21].
The TARGET7-module uses four TARGET7-ASICs (Application-Specific Integrated Circuit), each with 16 analog input channels. Furthermore, the TARGET7 uses an FPGA (Field Programmable Gate Array) which is responsible for the controlling of the four ASICs [20].

3.1 Characteristics of the TARGET7

The TARGET7 has a sampling rate of 1 GSa/s so that it can take one sample every nanosecond. The individual samples are arranged in an analog ring memory with 16384 memory cells. If the read out starts with the FPGA, the samples become digitized (see figure 3.2). Theoretically, it should be possible to read out waveforms with a length of 16384 ns. In practice, the TARGET7 is still in development and it is possible to read out 448 cells for one waveform with a length of 448 ns [20].

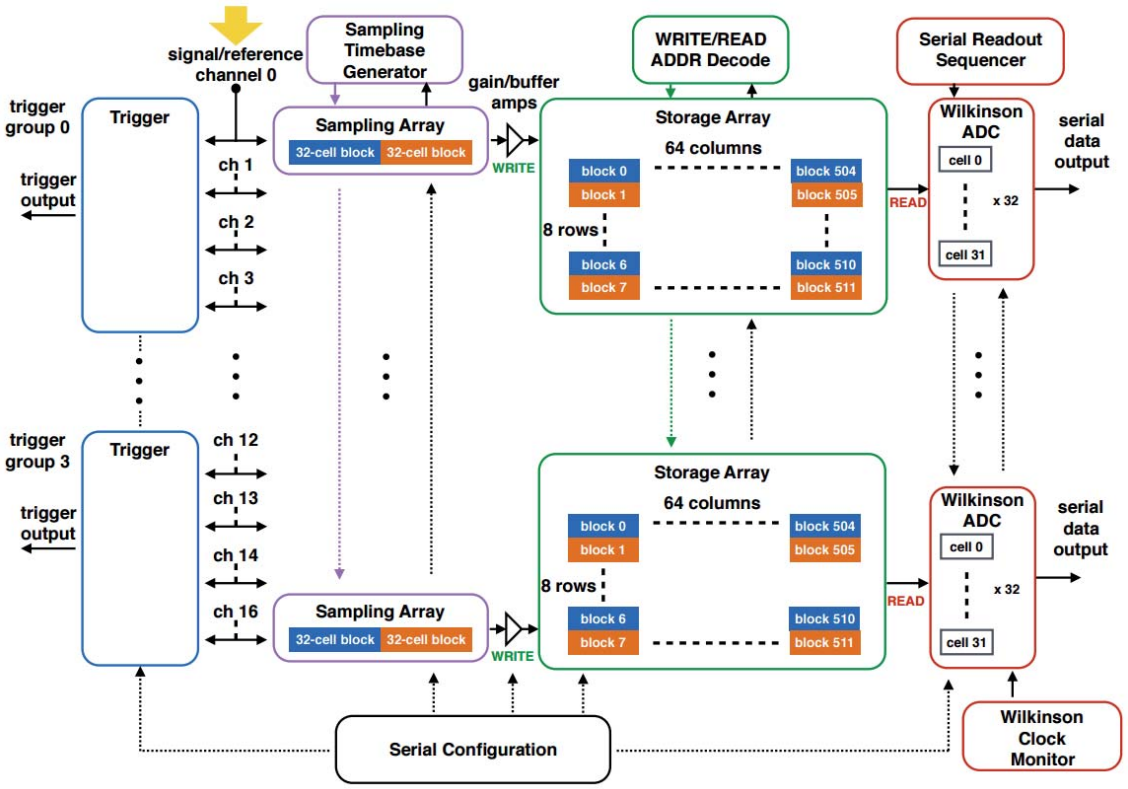

Figure 3.2: Functional block diagram of the TARGET7 ASIC [22]. Firstly, the samples are stored temporarily in a memory which can catch two blocks of 32 samples (sampling array). If one of the blocks is full, the block is given to the store array which includes 512 of these blocks. It is possible to measure continuously, because the two blocks of the sampling array are alternating. The 512 blocks with 32 samples are used in sequences so that the memory works like a ring buffer. When the FPGA asks for the samples, they are digitized by an ADC, 32 samples at once. After the digitisation they are read out in the 32 sampling blocks [22].

The analog input of the ASICs consists of a signal pipping and a reference pipping. With the reference pipping it is possible to set a DC voltage pedestal (Vped) to the channels. The Vped corrects the DC voltage part of the signal and lifts the baseline of the measurement. If there shall be measured a negative voltage with the TARGET7, it is important to set the Vped, because the Analog-to-Digital Converter (ADCs) is not able to handle negative voltages. If the baseline is lifted up, the ADCs get a positive value and they can digitize the data. The offset has to be considered in the evaluation.
Preamplifiers are included in the TARGET7-module which amplify the input signal before it is digitized. The Preamplifier also acts as a bandpass filter so that they change the real signal. It seems that the bandpass filter works like a differentiator, this can be seen in chapter 3.3.2.
Only the trigger signal can initiate the read out of the samples. Accompany, the digitization and the transmission to the computer starts, so that the data can be analysed. The different types of the trigger are explained in chapter 3.3.

3.2 Commissioning of the TARGET7

3.2.1 Hardware for the TARGET7

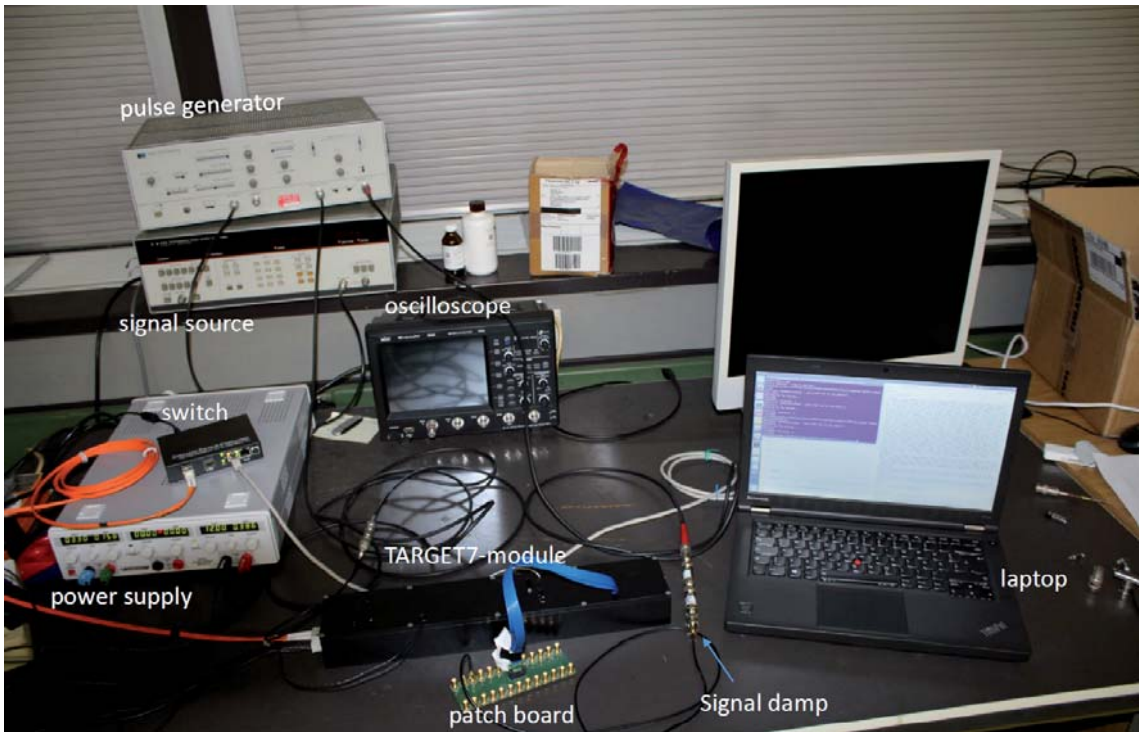

Figure 3.3: A possible measurement set-up with the TARGET7-module for understanding the trigger types. In this set-up the TARGET7-module is connected to the patch board, the switch (Ethernet Switch Converter 10/100/1000 Base-Tx to 1000Base-Fx) which is connected to the laptop, and the power supply (TRIPPLE POWER SUPPLY HM7042-2). Channel 0 of the patch board is connected over two signal damps (J01006A0837) to the inverted output of the 8082A pulse generator from Hewlett Packard. The normal output is connected to the external trigger input of the TARGET7-module. The pulse generator is triggered with the 8165A programmable signal source 1mHz - 50MHz, also from Hewlett-Packard.

A picture of the hardware and how it is connected can be seen in figure 3.3. The TARGET7-module needs 12 V as main voltage and 3.3 V as supply voltage. The power supply generates the voltage for the TARGET7-module (figure 3.3). The TARGET7-module has a network interface so that a local area network (LAN) for the data transmission and for the communication can be used. Therefore, the Laptop and the TARGET7 are connected to the same network switch, separated from the normal RWTH network. This is only a precaution measurement because the TARGET7-module has a static IP address. It is not possible to assign the TARGET7-module another IP address. Furthermore, the IP address can not be in use by other units in the same network.

The TARGET7-module is also connected to the patch board with a ribbon cable. Theoretically four patch boards could be connected to the TARGET7-module, each with 16 SMA ports for a read out of 64 channels. In practice there is only one patch board with 16 SMA ports available which is absolutely sufficient for understanding how the TARGET7-module works. One of the SMA ports is connected to the inverted output of the trigger generator for testing measurements of the trigger delay (chapter 3.3.2).

3.2.2 Software for the TARGET7

The software of the TARGET7 for the communication and the data capturing was developed and provided by the CTA consortium, partly modfied by Erik Ganster in the course of his bachelor-thesis [20]. The software is written in C/C++, but it is possible to use all functions of the software in python, due to a Software-Wrapper. All programs are installed and used on a RWTH laptop with Ubuntu, version 16.04LTS [20].
For this bachelor-thesis the most useful program is the program "takedata.py". This program includes all necessary steps for taking data with the TARGET7-module. For example it includes the packets target_driver for the communication with the TARGET7 and target_io for the data acquisition. Furthermore, it is possible to customize the settings like the Vped or the trigger mode. The program reads the data out and saves it on the computer as a fits file. Fits files are compact file forms developed by the NASA which are supporting multidimensional arrays [23]. After the data is written down, the laptop disconnects itself from the TARGET7-module and the TARGET7 stops sampling.
For the different settings the program is modified and saved with new names by Benjamin Pestka, so that the TARGET7 can be used more easily and the code has not to be changed every time. An example is the program "takedata_warm_machen.py" which lets the TARGET7-module measure without writing the data down. During the measurement, the TARGET7-module heats up until it has a nearly constant temperature which is depending on the environment. Mostly, the temperature stays constant when it reaches a temperature between 55 °C and 60 °C. It depends on the outer temperature and the material, on which the TARGET7-module is standing. For example, it heats up faster on a wood desk than on a desk made of a more heat conducting material. It is important for the measurement that the temperature is constant because the given value from the TARGET7-module is correlating with the temperature (see the bachelor-thesis by Erik Ganster [20]).
For controlling the temperature is also implemented a program in the initial software. During the measurement the temperature should be checked several times for calibration reasons.
All the modified programs are stored on the RWTH laptop, as well as a read_me file.
Programs for the evaluation of the TARGET7 data made by Erik Ganster during his Bachelor-thesis and programs made by Nina Höflich or by Nina Höflich and Benjamin Pestka for the evaluation are on the laptop as well.

3.3 Data acquisition with the TARGET7-module with the different types of the trigger

The principle set up for a measurement with the TARGET7 can be seen in figure 3.3. The first ones are noise measurements without any modules connected to the channels. This measurements are done for the understanding how to measure with the TARGET7-module.
As already mentioned in chapter 3.1, the read out of the samples starts with the trigger signal. There are three different settings for the trigger which can be set in the program "takedata.py" for starting to read out the samples. In the following will be explained how the different trigger types work and will be done an appraisal how good the trigger works.

3.3.1 The Hardsync Trigger

The first tested trigger mode is the hardsync trigger.
The hardsync trigger takes the data with a constant frequency of about 120 Hz. A measurement with the hardsync trigger starts always at the same first cell [20]. This characteristic, in combination with the trigger delay, is advantageous for calibration measurements. It is possible to choose the first cell of the read out, by setting the right trigger delay. This allows to get a lot of data for all cells of the ring buffer. The maximum value of the trigger delay is equal to the number of cells, so that the maximum trigger delay is 16383 ns. The first cell of the read out and the following data are correlated, this must be considered. More details about the correlation of the first cell and the following data can be found in the bachelor-thesis of N. Höflich [19]. A disadvantage is the time which is needed to make specified measurements for all cells. As solution is the calibration measurement with the external trigger in a shorter time, but also with less data. It depends on the situation, which measurement for the calibration is better.
It is possible to make measurements with the hardsync trigger, but it is not the best choice for a measurement with the FAMOUS telescope to see Cherenkov light or fluorescence light. It is not useful to make measurements which takes only 448 ns, irrelevant if there is a shower or not. This would cause a huge data volume of information, most of it filled with noise. Furthermore, there can be missed events during the time when the TARGET7-module does not trigger. It would be just fortune to find good results with the hardsync trigger.
In conclusion, the hardsync trigger can be used for the calibration measurement, but it is not advisable to make measurements for detection of air showers with the hardsync trigger with the FAMOUS telescope to detect air.

3.3.2 The External-Trigger

When the external trigger is in use, the TARGET7 waits for a signal on the external trigger input, before it starts to read out the data. The external signal has to be at least 8 ns long and it must have at least a voltage of 2 V [20]. This is in accordance with the trigger output signal of the hardsync trigger (figure 5.2 in the appendix).
Otherwise than by the hardsync trigger, the external trigger starts at different cells with reading out the data, and this fact has to be considered foe the calibration. For this reason it is possible to get the information about the first cell of every measurement. This means that it is possible to assign every sample to the cell which measured the sample [20].
It also has to be considered that the standard settings of the trigger delay is not optimized for the measurement with the FAMOUS telescope or a pulse generator. With the standard settings it is not possible to see the original pulse which caused the measurement. Therefore, the trigger delay must be set up for example at 424 ns, so that the pulse can be seen well on the recorded data. To determine the right trigger delay, there were made measurements with the set-up which is shown in figure 3.3.
For a signal which fulfils the requirements for the external trigger of the TARGET7, the signal of the pulse generator was tested on the oscilloscope, which can be seen in figure 3.3, too. Another method to test the signal, is to start the measurement and if the written file is empty, the trigger signal did not fulfil the requirements. It would be advisable first to control the signal with the oscilloscope because it is much easier to assess how much the signal has to be changed for good measurements. The pulses were sent with the pulse generator with a frequency of 10 Hz. To be sure the pulse at the trigger signal and at the patch board are coming in at nearly the same time, the signal for the patch has to come from the same pulse generator, in an inverted way at the same time. The pulse generator uses BNC ports, while the external trigger input of the TARGET7-module uses Lemo ports, so there was used a Lemo-BNC-adapter. For the patch board with SMA ports, there was also needed an adapter, from SMA to BNC, as well as two signal damps, each with a damping factor of 20 dB.

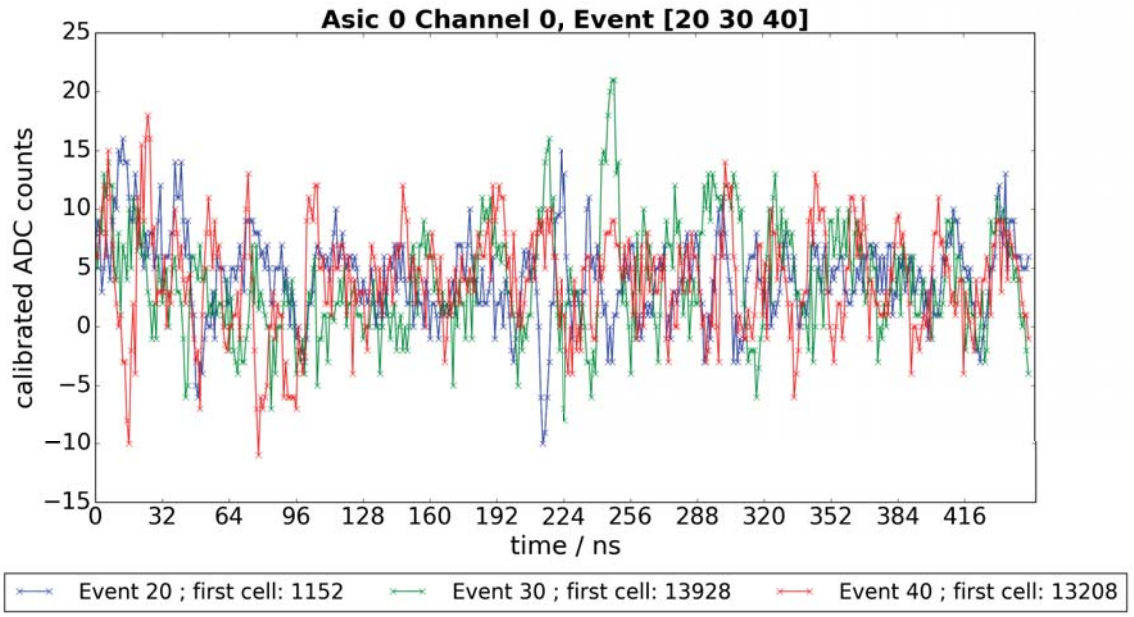

Figure 3.4: Here can be seen a trace of the noise, measured with the TARGET7-module, without anything connected, triggered with the external trigger. The baseline is corrected. Because of another temperature of the TARGET7-module during this measurement and the measurement for the calibration, the baseline fluctuate at five ADC counts instead of 0. In this measurement, there is no problem because the measurement shall show how the baseline principally looks like. In this plot three different traces are shown, of three different events, the events 20, 30 and 40. One event means, that the trigger got one signal and it starts counting at 0, so that the 20th event is the 21st time that the trigger got a signal in this measurement. The first cell gives the starting point of the ring buffer, where it starts to write out the samples.

Firstly, there is shown in figure 3.4 a trace without the signal at the TARGET7-module for comparing it with the signal from the pulse generator. Figure 3.5 shows the trace with the signal and standard settings for the trigger delay. As can be seen, no pulse signal is in this trace. A reason could be, that the pulse signal is so small and disappears in the baseline. However, it is noticeable in figure 3.6 that the signal is much higher than the baseline. In figure 3.6 the trigger delay is set at 424 ns and the signal is clearly recognizable. Because of the relative small frequency of 10 Hz, compared to the length of the trace, it is most likely the same signal which caused the trigger.
If the trigger delay is set greater, the buffer is read out in an earlier cell, so that the signal moves right (compare figure 5.5 in the appendix). As it can be seen, there should be used a trigger delay of 400 to 600 ns for measurements with the external trigger.
Moreover it is distinguishable in figure 3.6 that the TARGET7-module changes the signal. The traditional signal was an inverted rectangle pulse (see figure 5.3 in the appendix) and the TARGET7-module shows the signal after the band-filter.
In conclusion, it can be said that the external trigger of the TARGET7-module works well and gives good results. This trigger mode was also used in the measurements with the FAMOUS telescope (see chapter **??**).

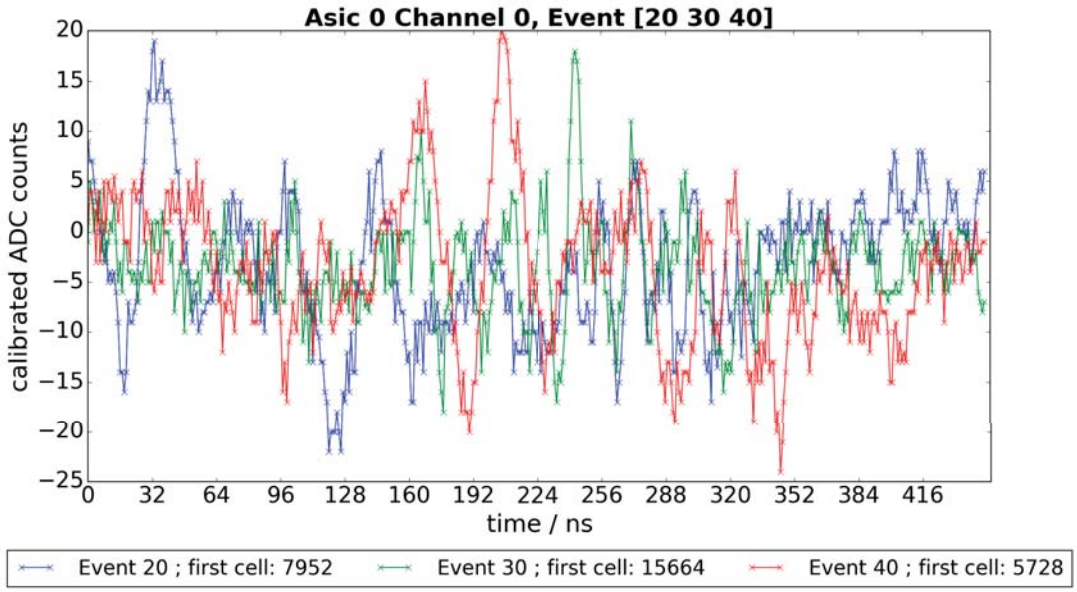

Figure 3.5: Here can be seen a trace, measured with the TARGET7-module, triggered with the external trigger. The same signal which is used for the external trigger is send to channel 0 in a debilitated way, like explained in the text. The trigger delay is not changed so that the standard settings are in use. As it can be seen, the signal is in principle the same as in figure 3.4. There is an oscillation in event 20 and 40, but these are not from the pulse generator, these oscillations comes from the location where it was measured (Halle Physik RWTH Aachen, Germany). On this place is a known phenomenon which cannot be shouted down. The sent signal which caused the measurement cannot be seen with the standard settings of the trigger delay.

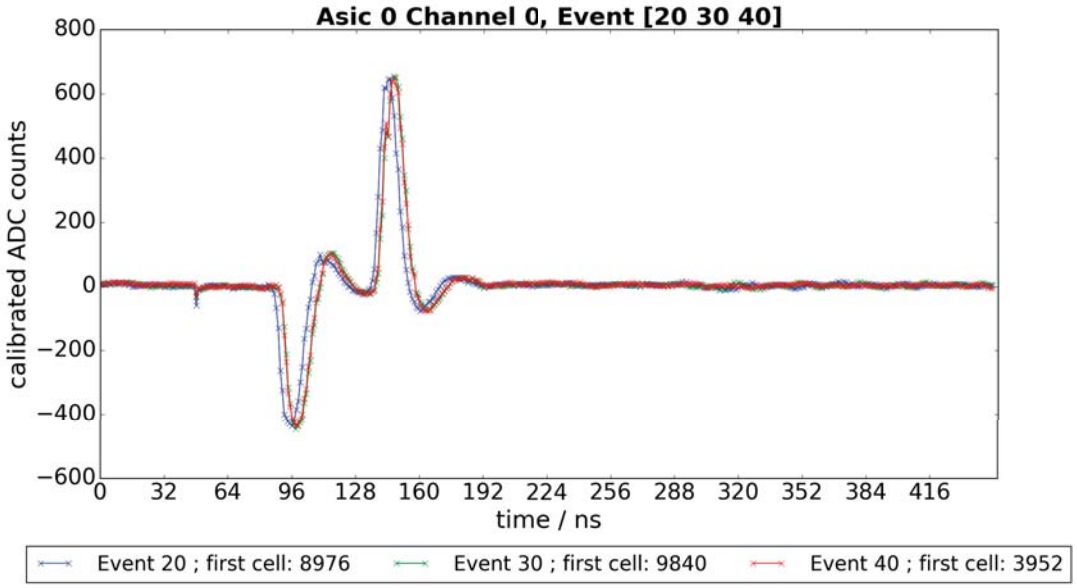

Figure 3.6: Here can be seen a trace, measured with the TARGET7-module, triggered with the external trigger. The same signal which is used for the external trigger is sent to channel 0 in a debilitated way. The trigger delay is set at 424 ns and it can be seen well with an amount of 600 ADCcounts or rather by −400 ADCcounts. The signals seems to be the derivative of the signal input, which is a square-wave signal (nearly the same signal like in figure 5.4 in the appendix).

3.3.3 The Self-Trigger

The third trigger mode which can be used is the self trigger. The self trigger allows to trigger directly at the incoming signal. Therefore, four channels are combined as a trigger group. The sum of the trigger group is compared to a given threshold and if the sum exceeds the threshold, the trigger causes a read out. The self trigger is explained in detail in chapter 3.4.

3.4 Commissioning of the Self-Trigger

The motivation to active the self trigger of the TARGET7-module is to use it during night measurements with the FAMOUS telescope to detect Cherenkov light or fluorescence light of air showers.
Every ASIC of the TARGET7-module consists of four trigger groups. Every trigger group consists of four channels. The first group of the first Asic ("the first ASIC" is equal to "ASIC 0", the same principle for the first group) implements the channels zero to three, the second group the next four channels and so on. The system triggers to the sum of the four channels of a trigger group. The triggers are connected to the FPGA and can cause a read out of the TARGET7. Every trigger group can be set on and off individually [24].
There are two parameters for the self-trigger which can be set: The threshold and the PMTref4 [24]. Both parameters are DAC values (digital analog converter) and each DAC count should be equal to 0.601 mV. The parameter PMTref4 sets the reference voltage for the sum of the trigger and will be added to the sum of the four channels. The PMTref4 can be set up for every trigger group individually. The range of the PMTref4 is from 0 to 4095 ADC counts.
The second parameter of the self trigger is the threshold which also has a range from 0 to 4095 ADC counts. The threshold is a reference voltage for the digital trigger output for the sum of the trigger groups, it can be set for every group individually. When the sum of the trigger group exceeds the given threshold, the TARGET7 starts to read out the data. The threshold has to be calibrated first, so that there can be adjust a reasonable threshold. Therefore, it should be done a 2 D-scan for the two parameters, the PMTref4 and the threshold. For the scan should be put different signals on the trigger groups and measure the trigger efficiency. After the measurements for one PMTref4-threshold-pair, the efficiency can be plotted against the amplitude and fitted a Gaussian error curve. The standard deviation and the mean of the fit are values for the noise and the threshold. This procedure has to be done for the different PMTref-threshold-pairs. The results have to be written down in a 2 D histogram and then there can be seen which PMTref-threshold-pair gives the lowest noise [24].
Before the 2 D-scan can be started, there has to be tuned the offset level of the channels among themselves and to the PMTref. The offset can be set up with the two parameters Vofs1 and Vofs2, for each channel. A calculation of the Vofs are done by the program "TuneNodeABC.py" which was given in the primary software. The program checks the difference between the offset level and a specific value of the TARGET7 (in the program called targetV). If the difference is higher than the given tolerance, there is set up a new Vof-value and checked again. This procedure is made for both Vofs, for each channel. Furthermore, the PMTref is also tuned for each group. This means, that the 2 D-scan can be made around the given value.

Because of the dependence of the baseline, the Vofs and the PMTrefs has to be tuned for every Vped individually which affects the position of the baseline.
The program had to be modified in several ways, so that it can tune the Vofs and the PMTrefs now. Before modifying the program, the values for the Vofs and PMTrefs were given out like it can be seen in figure 3.7.

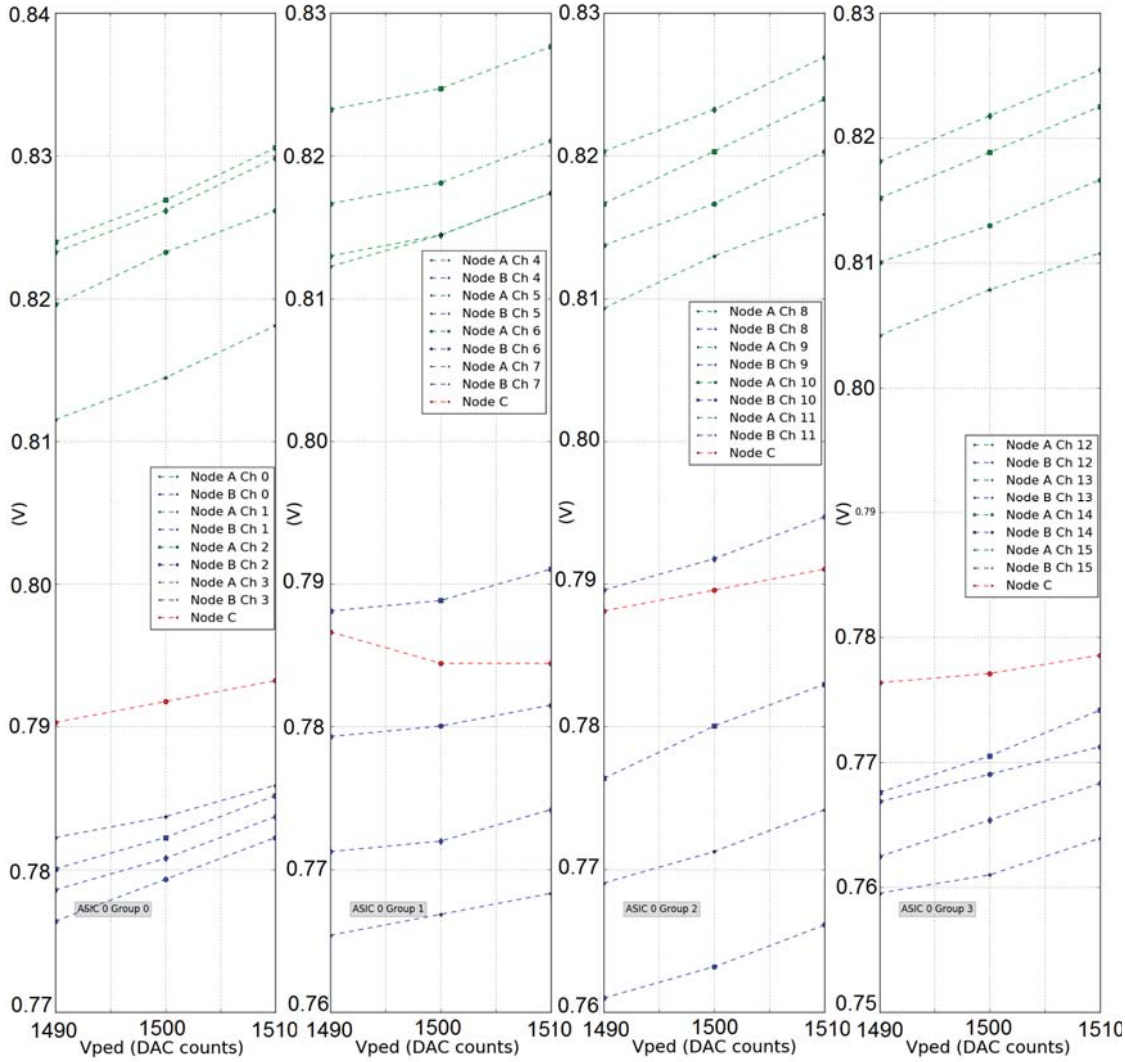

Figure 3.7: The results of the tuning program for the tuning of the Vofs and PMTrefs for 16 channels for the self trigger. The exact values are written down in a text document.

After tuning the Vofs and PMTrefs, there should start the already described 2 D-scan for the optimal PMTref-threshold-pair. Therefore, the given PMTrefs and the Vofs were set in the "takedata.py" program, as well as a low random threshold. To get an impression for the value of the threshold, there are done noise measurements without anything connected to the TARGET7. To see at which threshold the baseline can not cause a trigger signal anymore, the threshold is increased every time when the TARGET7 gets a trigger signal because of the baseline. During this measurements two problems arose.

The first problem is the fact, that the TARGET7 triggers at every threshold-level. If the highest possible threshold of 4095 DACcounts is set, the TARGET7 still reads out the baseline. At this point it is remarkable, that the TARGET7 does not trigger constantly. The number of events is not constant, which may mean that there could be a signal in the baseline which causes the read out. A look at the taken data shows some spikes during the measurement with the self trigger (figure 3.8).

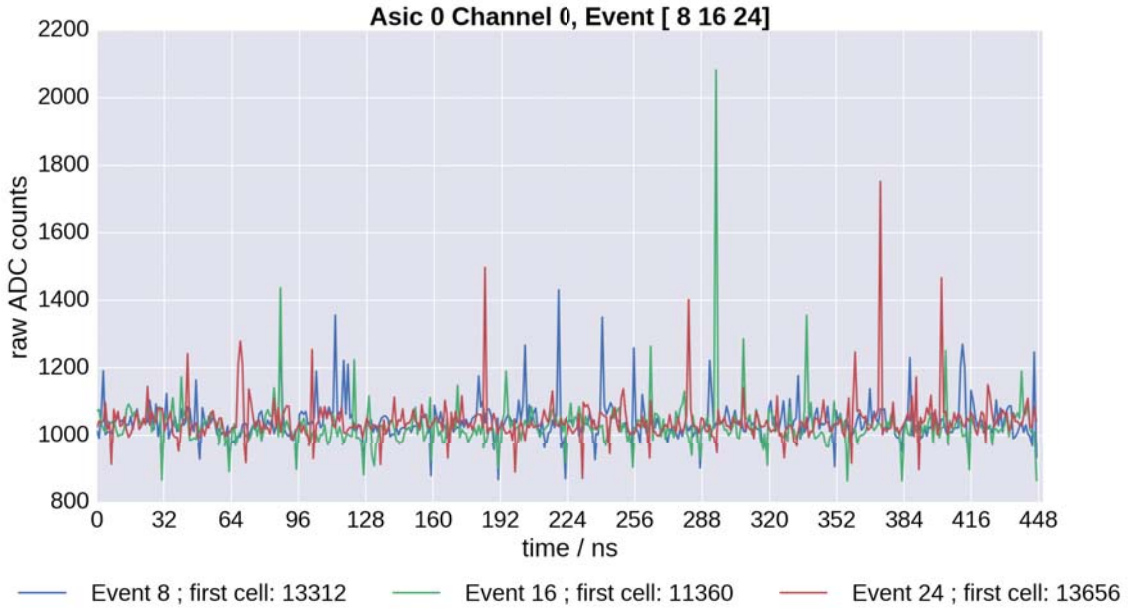

Figure 3.8: Here can be seen three traces, three events of a noise measurement with the self-trigger of the TARGET7-module. Here is nothing connected to channel zero or to any other channel of the TARGET7-module and the threshold is set at the maximum of 4095 DACcounts. As can be seen, there are spikes with an amount of up to 1000 ADC − counts over the baseline, without a sensible reason.

In order to better assess, if the spikes would be the reason for triggering, there are done more investigations. The trigger is set only for the first trigger group, the threshold is set at the maximum and the channels are not connected, so that it is a noise measurement again. The baselines are corrected with the calibration-program from N. Höflich [19]. After the calibration, the signals of the channels are summed up. The sum is plotted and analysed, if there is a spike in the area where the signal for the trigger should be, when the trigger delay is set to 424 ns. As it can be seen exemplary in figure 3.9 and 3.10, sometimes there are spikes which could cause a trigger and sometimes there is only the noise of the baseline which has no chance to be the reason for triggering. This could be an evidence that the TARGET7-module trigger randomly because of a possibly wrong readout or information transfer during the use of the self trigger. If this should be true, the software of the TARGET7 should be revised.

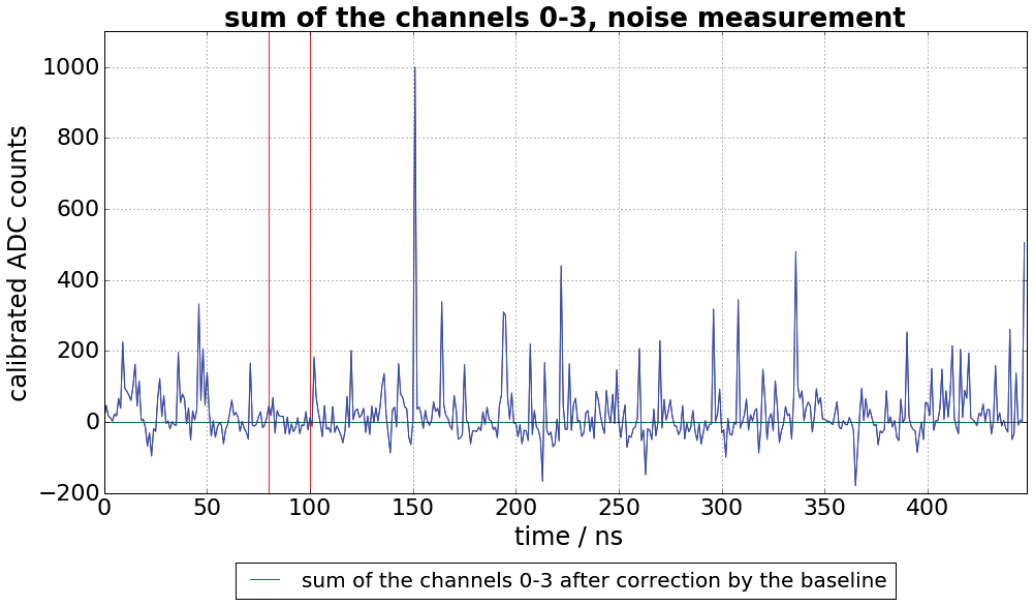

Figure 3.9: Here can be seen a sum of three calibrated traces, the traces of the channels zero to three. All traces are taken with the TARGET7-module, using the self trigger with the highest possible threshold without anything connected to it, a noise measurement. The trigger delay is set to 424 ns, so that the signal which caused the read-out should be in the area between the two red lines. As it can be seen, in the area is only small noise. 60 ns later can be seen a high peak, but this peak could not cause the trigger anymore.

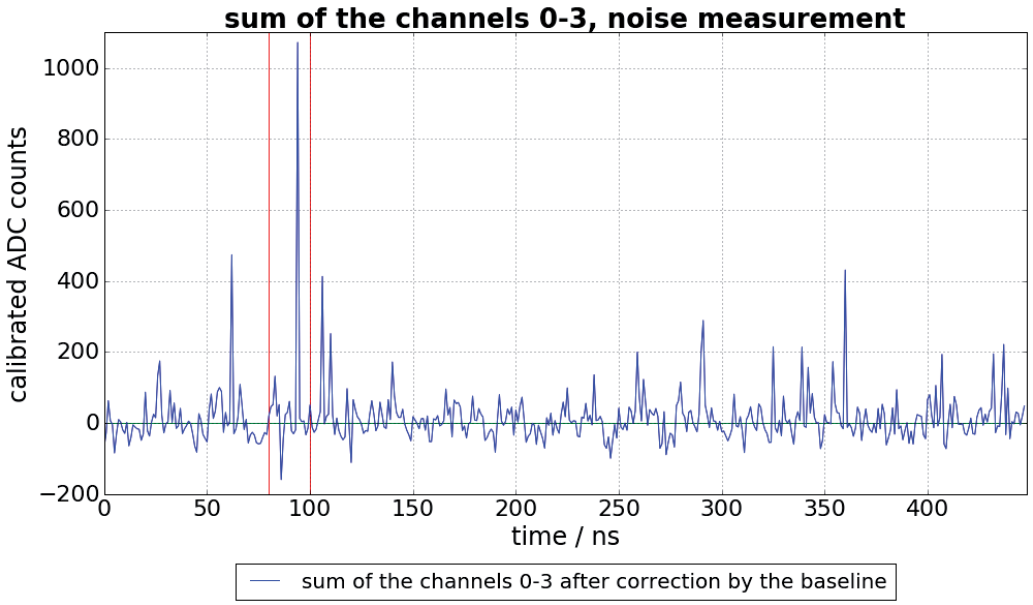

Figure 3.10: Here can be seen a sum of three calibrated traces, the traces of the channels zero to three. All traces are taken with the TARGET7-module, using the self trigger with the highest possible threshold without anything connected to it, a noise measurement. The trigger delay is set to 424 ns, so that the signal which caused the read-out should be in the area between the two red lines. This time, there is a height peak in the area, but not 60 ns later as in figure 3.11.

For better assessment, there is also done a measurement with a similar experimental set-up as it can be seen in figure 3.3. In this measurement there is no signal given to the external trigger input. Besides, the given signal on channel zero is not inverted this time. The pulse is sent with the pulse generator with a frequency of 10 Hz. This measurement shall check if the given signal is at the right place to cause a read out as a trigger signal. Therefore, the trigger delay is set to 424 ns, so that the signal should be in the same place as in figure 3.6 of the measurement with the external trigger delay. These measurements are done under the assumption that the trigger delay has to be set up in the same way as for the external trigger. Nevertheless, there are done measurements with other trigger delays up to 600ns, for testing if the trigger delay needs other set ups for the self trigger.

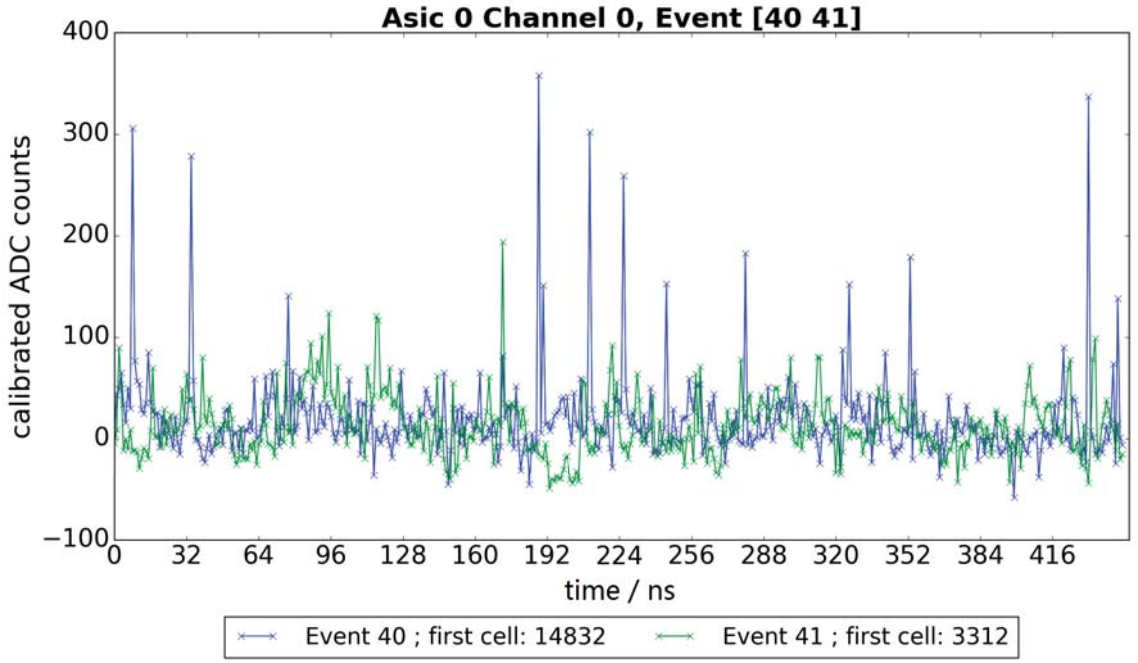

Figure 3.11: Here can be seen a trace taken with the TARGET7-module, using the self-trigger with the highest possible threshold and a trigger delay of 424 ns. A square-waveform signal with a frequency of 10 Hz is given to this channel, like it can be seen in figure 5.4. In this trace nothing can be seen, which is caused by this pulse, only the normal baseline during a measurement with the self-trigger.

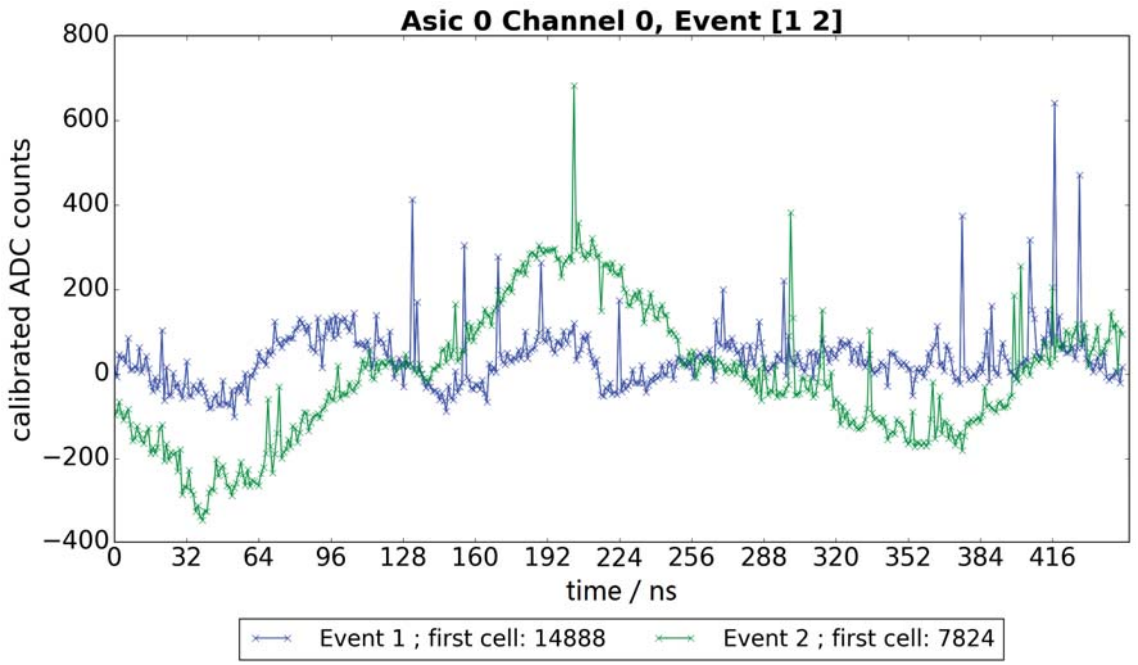

Figure 3.12: Here can be seen a trace taken with the TARGET7-module, using the self-trigger with the highest possible threshold and a trigger delay of 424 ns. A square-waveform signal is given with a frequency of 10 Hz to this channel, like it can be seen in figure 5.4. The data oscillate with a frequency of about 30 MHz. The characteristic peaks of the self trigger are still there.

The measurements have shown, that the self trigger does not react at the pulses which are sent to the channels. The pulses did not cause the trigger, as can be seen in figure 3.11. Furthermore, there should be 600 events in a measurement which takes 60 seconds, instead there are only 80 events. On the other hand, there are sometimes oscillations like shown in figure 3.12 which are not there, when the pulse generator does not send signals. The problem for understanding is, that the frequency and the form of the oscillation do not fit to the given signal so that it is not known, where the signal comes from. There must be other interfering signals than the known signals.

The second problem during a measurement with the self-trigger of the TARGET7-module is a memory error which appears after exactly one measurement. It makes no difference if the measurement takes five minutes or only ten seconds. After the program determines that the measurement is finished, appears an error. Furthermore, it makes no difference if the TARGET7 shall make only one measurement or more measurements in a row, the error appears after the first one. When this happens, the TARGET7 has to be rebooted. At least one, maybe more settings are set back to the standard settings and they do not take the given settings, like for example the Vped. In figure 3.13a and figure 3.13b can be seen the difference between the first measurement and the second measurement with the self-trigger after the memory error and without rebooting.

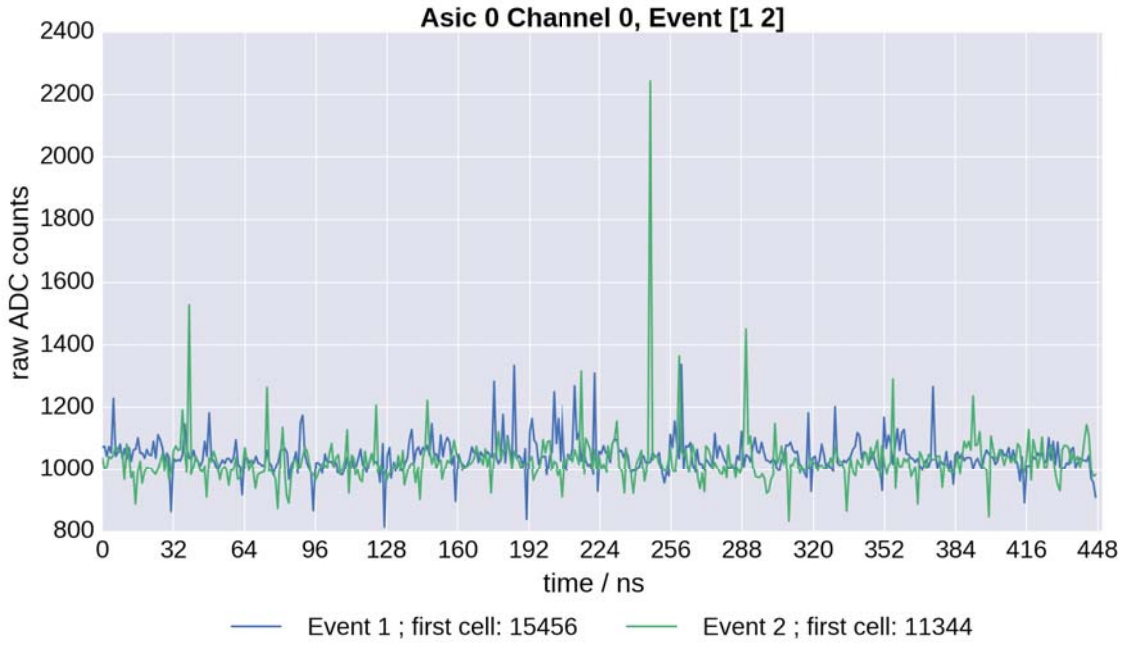

(a)

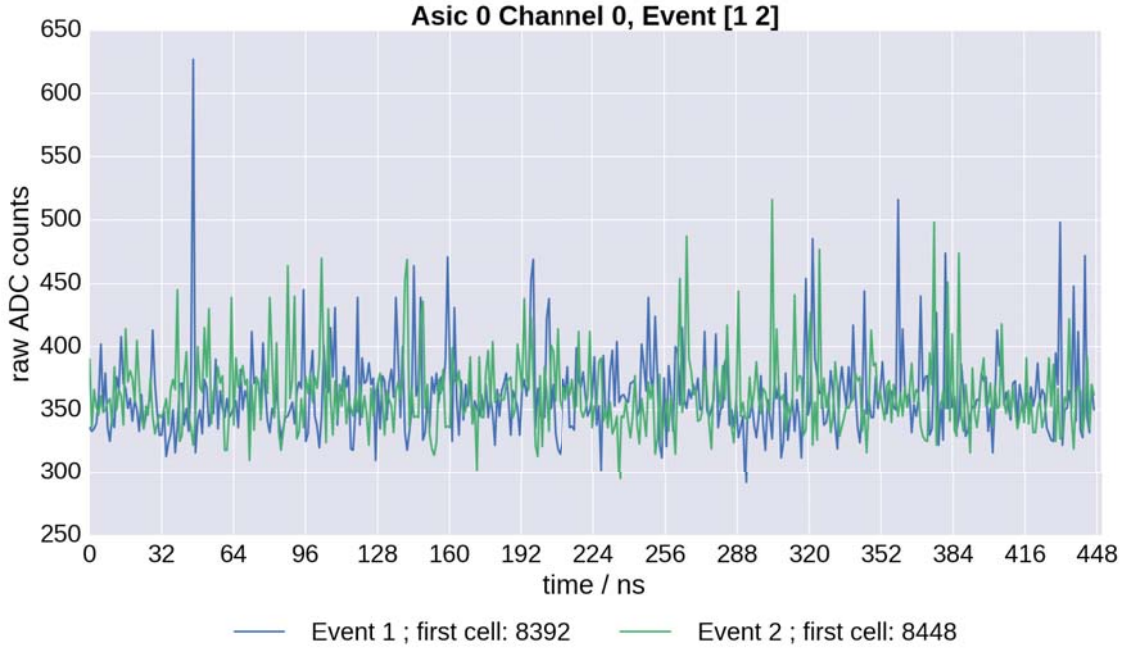

(b)

Figure 3.13: Here can be seen two traces taken with the TARGET7-module, using the self-trigger. These are two noise measurements without anything connected. The first trace is taken after the TARGET7-module is booted, the first measurement. The second trace is taken directly after the first one, without rebooting the TARGET7-module after the memory error was shown in the first measurement. As it can be seen, the baseline is shifted down, although the Vped should lift it up like it is seen in the first measurement.

As can be seen in figure 3.13, it is useful to reboot the TARGET7-module after every measurement with the self-trigger. Interesting by this memory error is the fact, that also a debugging program could not find the location of the error, where exactly the

error occurs. So it is very difficult to fix this error and it is not clear, which impact the error has on the data, except of the known effect after the first measurement.
In conclusion, there were done a lot of steps for understanding the self-trigger of the TARGET7-module and the knowledge could be acquired, what should be done before the measurement with the self-trigger starts. The first steps of the preparation for a measurement with the self-trigger of the TARGET7-module are completed successfully. Before the self trigger can be used for a measurement with the FAMOUS telescope, more steps have to be done.

4. Measurements with FAMOUS

This chapter deals with the measurements with the FAMOUS telescope. Dark measurements with the oscilloscope in the laboratory and field-measurements outside at night with the TARGET7-module. 20 of the 64 pixels are available for the measurements, just like said in chapter 1.2. All the measurements and the evaluation of the data were done in cooperation with Nina Höflich.

4.1 Measurement with the Oscilloscope

All the measurements with the oscilloscope are dark measurements made in the hall of physics in the physic center of the RWTH Aachen, Germany.
The measurements with the oscilloscope has been done for preparations for the real measurements with the TARGET7-module, before the TARGET7 was available for this bachelor-thesis. The preparations include programs for the evaluation and the knowledge how to make measurements with the FAMOUS-telescope.

4.1.1 Set-up and data acquisition

The set-up for the measurements with the oscilloscope includes two computer, a LeCroy WJ354A oscilloscope, an amplifier board (built by J. Schumacher), a commercial power supply and the FAMOUS telescope. The FAMOUS telescope is connected via LAN to one of the computers which controls the power supply unit (PSU) via a program written by J. Schumacher. The program allows to check the temperature of every individual pixel, to read out the bias-voltage and to set the over-voltage for all of the pixels. For all of this measurements, the over-voltage is set at 1.4 V, the default value specified by the manufacture. Furthermore, whith the program it is possible to turn the bias-voltage on and off. One of the pixels is connected via the prepared SMA-cables to the amplifier. The amplifier is connected to the commercial power supply and with a SMA-cable and a BNC-SMA-adapter to the oscilloscope, which uses Ethernet for communication with the second computer. The second computer takes the data from the oscilloscope.
This set-up is used for all measurements with the oscilloscope. Each of the 20 pixels has been measured 2 x 100 times, so that there are 200 traces for every pixel. One trace includes $5 \cdot 10^5$ samples, one sample every nanosecond.

4.1.2 Evaluation

4.1.2.1 Integration over the SiPM-signals

Before starting the evaluation, one should have a closer look at the traces. In figure 4.1 can be seen, how the SiPM-signals looks like, when there are no interfering signals and how one whole measurement looks like.

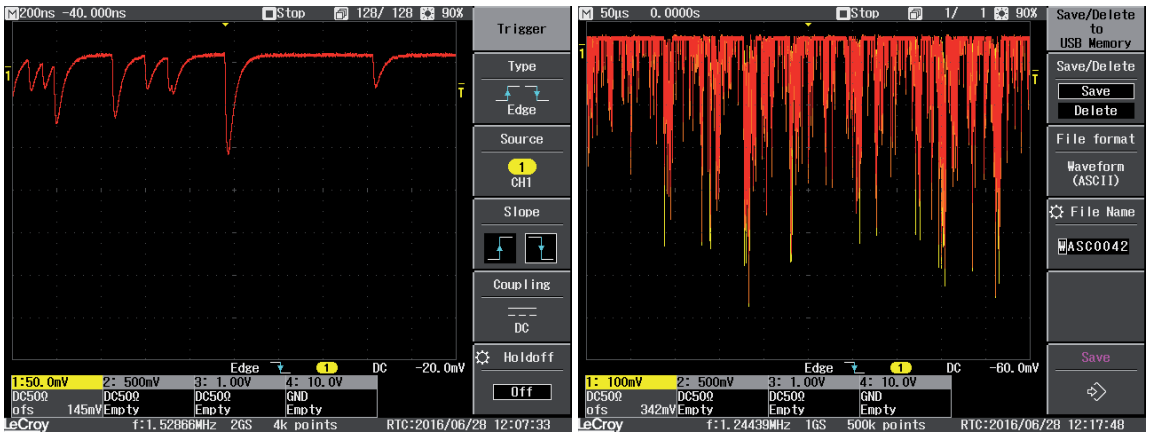

Figure 4.1: Both traces are taken with a LeCroy WJ354A oscilloscope while it is connected to SiPMs in the FAMOUS telescope over an amplifier, during a dark measurement. The left trace shows the individual SiPM-signals, how the different p.e. signals look like. Here can be seen the 1 p.e., 2 p.e. and 3 p.e. signal, they can be separated by the different heights. The x-axis shows the time-line, one box stands for 200 ns. The y-axis shows the measured voltage, one box stands for 50 mV.
The right trace shows how one whole measurement looks like, with $5 \cdot 10^5$ samples. There can be seen some very high p.e. signals. The x-axis shows the time-line, one box stands for 50 μs. The y-axis shows the measured voltage, one box stands for 100 mV.

The right trace in figure 4.1 is only one of the 100 measurements for every pixel. For the determination of the *gain*, the SiPM-signals has to be extracted from the trace and analysed. So it is necessary to implement an algorithm which extracts the SiPM-signals, integrate over them and consider the background and interfering signals, like the characteristic noise signal of the laboratory.
For the algorithm are taken some ideas of the program from C. Günther [25]. Firstly, the trace is flattened, the average of five neighboured samples is calculated. After the flattening a peak-finder program of M. Duarte is used, which can be found online [26].
The peak-finder algorithm compares the y-value to the values around to detect peaks. It is possible to detect positive and negative peaks, both with a minimal or maximal heigh, depending if there shall be found positive or negative peaks. Furthermore, the minimal distance between two peaks can be set. For detecting the SiPM-signals, the peak-finder shall detect negative peaks with a maximal heigh of -0.02 V and minimal distance of 20 ns. With the maximal height of -0.02 V there can be detect all peaks, also the 1 p.e. peaks. Unfortunately, the peak-finder detects also noise or the characteristic electric noise in the hall of physics which is already mentioned in chapter 3.3.2. For that reason there are filter implemented in the next steps of the algorithm which will be discussed later. The minimal distance between of 20 ns is

chosen because of double-detection of one peak. This means that the peaks are not always flat and there can be two maxima in one peak which would be both detected. To prevent the double-detection, the minimal distance is chosen to 20 ns. The chosen value has another advantage: It also prevents the detection of afterpulsing because the integration algorithm is not designed for afterpulsing.
For the following analysis, there are used the original data, not the averaged data. The detected peak-positions are used for the next step, the integration over the peaks. The integration algorithm implements filters for mis-detections, similar to the filter made by C. Günther [25]. The peak must fulfil the criteria of a negative value and a minimum negative slope at the steep slope of a SiPM-signal. The slope is calculated as a mean slope between voltage-value at the peak position and the voltage value which was measured 20 ns before the peak. The height difference must be at least -0.03 V, otherwise the filter does not count the signal as a SiPM-signal. Figure 4.2 shows the result of the filter. The red and the black points are detected by the peak-finder program, while the red ones are the peaks which passed the filter. The integration of the peaks begins after the filter. The integration area shall include

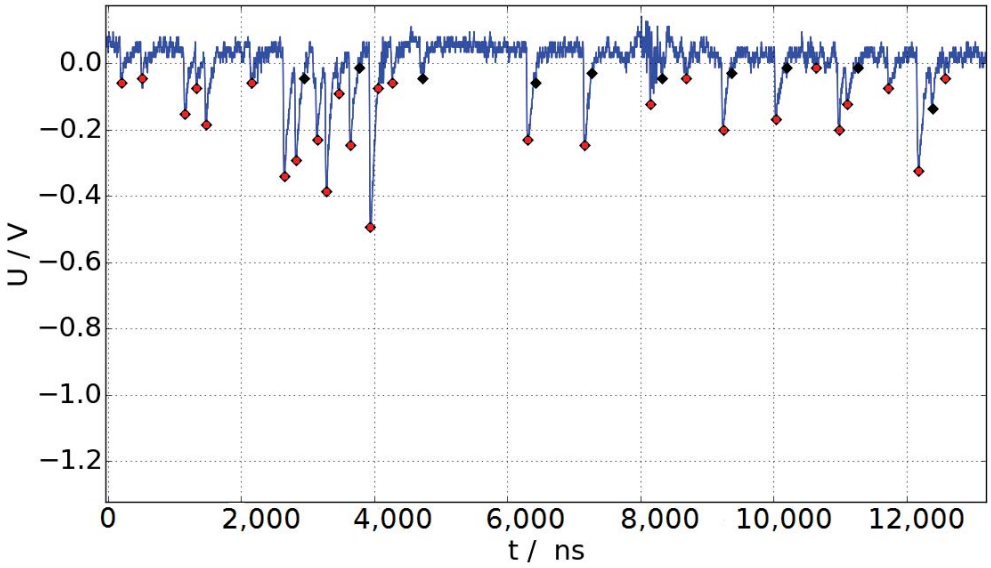

Figure 4.2: The trace is taken from the measurements with the oscilloscope of the central pixel of the FAMOUS telescope. Here can be compared the detected peaks before and after the filter of the integration algorithm. The red points are the detected peaks with the peak-finder which pass the filter, the black ones are the detected peaks which are sorted out. The filter does not work perfectly, sometimes it misses a 1 p.e. peak or detects the characteristic electronic noise of the hall of physics, but all in all the filter and the peak-finder work well together [19].

most of the steep slope and a bit of the slower decline (positive slope). Therefore the integration area is set to 20 ns before the peak position and 20 ns after the peak position. The 41 values are added and corrected by the baseline. The values from 30 ns to 20 ns before the peak are added and used for the correction of the baseline. The sum of the values for the baseline-correction is adjusted to the length of the integration area and subtracted from the integration. The resulting value is the used integral for the following analyses. Figure 4.3 shows the integration area of some SiPM-signals.

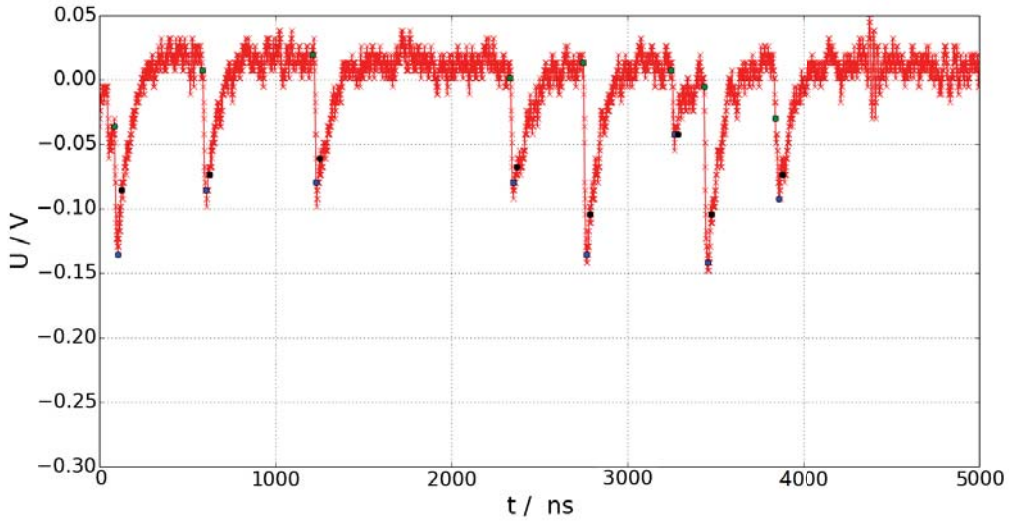

Figure 4.3: The trace is taken from the measurements with the oscilloscope of the middle pixel of the FAMOUS telescope. The integration area of the SiPM-pulse is marked with the green and the black points. The blue point is the founded peak by the peak-finder program.

4.1.2.2 Determination of the Gain

Integration over the SiPM-signals was done for all SiPMs connected with cables, two times 100 measurements. In the following, only the determination of the *gain* for the central pixel is presented and the important values for the other pixel are attached in the appendix (table 5.1 and 5.2).
The integrated pulses are negative values. For visual reasons, the values are multiplied with -1. The new values of the integrated pulses are filled into a histogram (figure 4.4).

Individual Gauss-fits

The logarithmic scale of the histogram allows to see the "fingers" up to high p.e. very well. The first try to determine the *gain* out of this finger-spectrum is to fit single gauss-functions to the first four peaks, because only the first four can be determined well. The fitted Gauss-function has three degrees of freedom, how it can be seen in equation 4.1.

$$f(x) = \frac{A}{\sqrt{2\pi\sigma^2}} \cdot exp\left(-\frac{(x-\mu)^2}{2\sigma^2}\right) \tag{4.1}$$

The parameter A is a measure for the amplitude, μ is the expected value of the integrated SiPM-signal and σ is the standard deviation. All parameters are optimized by the fit-algorithm. The results of the determination of *gain* with the individual Gauss-fits are not trustworthy enough, but they can be used as guide values for the analysis with the FACT-function. For more details, see bachelor-thesis of N. Höflich [19].

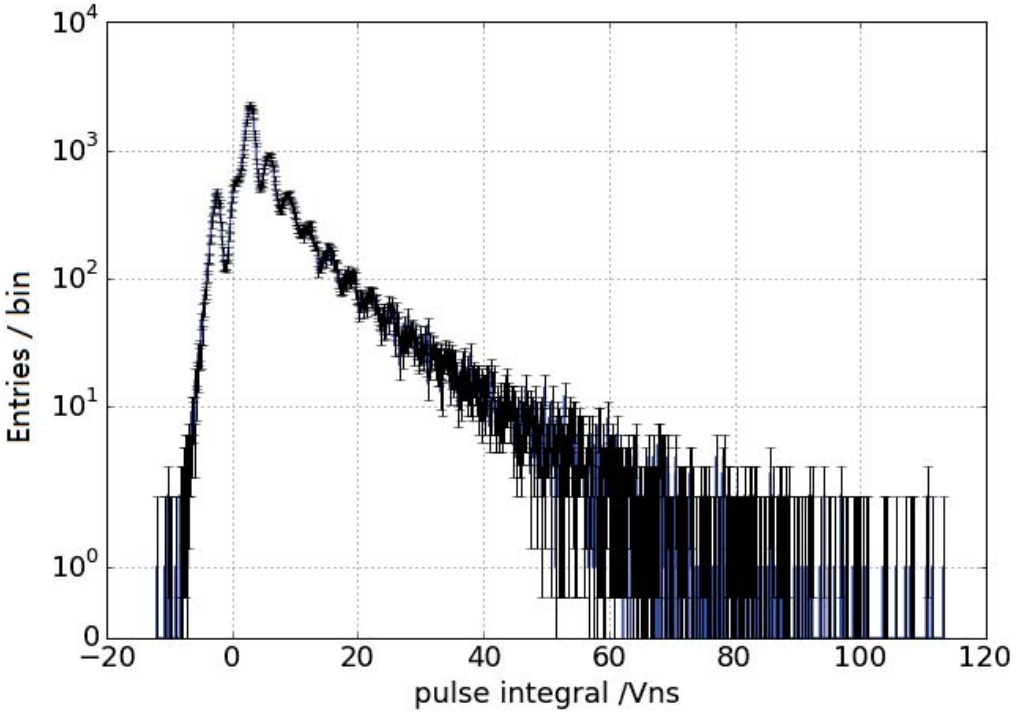

Figure 4.4: Histogram of the integrated SiPM-signals, multiplied with −1. The blue points are the absolute frequency of the calculated integral, the black bars are the errors which are adopted as Poissonian errors. The negative pulse integrals in the histogram are caused by the correction of the baseline, for example when the peaks of afterpulsing are detected. More details can be seen in the text. This figure is created together with N. Höflich [19].

FACT-fit

The analysing of the finger-spectrum can be made better by using the FACT-function, developed by the FACT collaboration for analysing the SiPM-finger-spectrum [27]. The Fact-fit considers the overlapping of the gauss-functions, the number of Gauss-functions, the crosstalk-probability, the *gain* of the SiPM and the width of the gauss-functions. Furthermore, there is multiplied the Erlang-distribution, for more informations, see paper [27]. The FACT-function can be seen in equation (4.2).

$$f(x) = A_{1\,\mathrm{p.e.}} \cdot \sigma_1 \cdot \sum_{n=1}^{N} \frac{exp\left(-\frac{1}{2} \cdot \left(\frac{x-x_\mathrm{n}}{\sigma_\mathrm{n}}\right)^2\right)}{\sigma_\mathrm{n}} \cdot \frac{\left(n \cdot p_\mathrm{fit} \cdot exp\left(-p_\mathrm{fit}\right)\right)^{n-1}}{(n-1)!^{\nu}} \tag{4.2}$$

With $A_{1\,\mathrm{p.e.}}$ as the amplitude of the first p.e. peak, σ_1 as the standard deviation of the first peak. N stands for the number of fitted gauss-functions and this should be equal to the number of fingers which can be seen.

The parameter x_n is the expected value for the nth Gaussian function with

$$x_\mathrm{n} = gain \cdot n + x_0 \tag{4.3}$$

with x_0 as the expected value for the p.e. peak. The σ_n stands for the standard deviation of the nth gauss-function with

$$\sigma_\mathrm{n} = \sqrt{n \cdot \sigma^2_\mathrm{p.e.} + \sigma^2_\mathrm{el}}. \tag{4.4}$$

$\sigma_\mathrm{p.e.}$ stands for the standard deviation of the produced charge in the cell and σ_el describes the fluctuation of the electric noise.
The second part of the sum of equation 4.2 is the Erlang-distribution. The parameter ν is the Erlang-parameter, p_fit is a parameter which is correlated with the crosstalk probability p_xt (equation 4.5).

$$p_\mathrm{xt} = (0.723 \pm 0.004) \cdot \left(\frac{p_\mathrm{fit}}{0.440106 \pm 0.00010} \right)^{\frac{0.875 \pm 0.005}{0.9515 \pm 0.0020}} \tag{4.5}$$

The correlation between p_fit and p_xt is found by simulations [27].
The FACT-fit has 8 parameters to fit, so that the algorithm needs starting values, where it shall search the best parameters.
The number of Gaussian functions N can be approximated by counting the fingers of the histogram. Therefore it should be said, that the area for the fit is chosen between 2.5 nVs and 50 nVs. The left limit is taken because of the asymmetry of the first peak resulting by noise, which has a bigger impact for the smaller signals. The right limit is taken because of the small rate of the higher peaks and the fact that some of the very high peaks are not detected completely by the oscilloscope and would adulterate the evaluation.
The other starting values for the parameters can be taken from the results of the evaluation with the individual Gauss-fits.

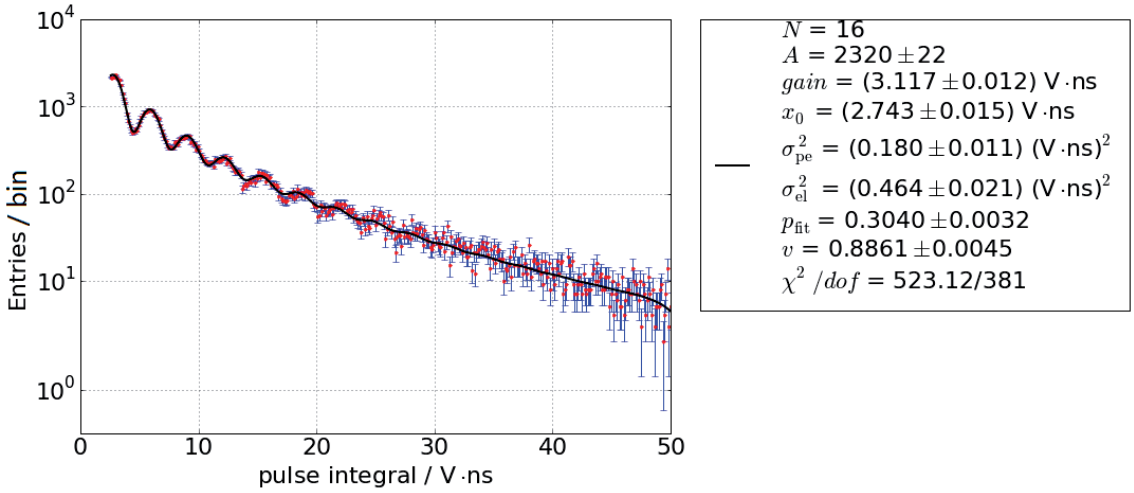

Figure 4.5: The FACT function fitted to the finger-spectrum in the area between 2.5 nVs and 50 nVs. The found parameters are in the box at the right side of the figure. This figure is created together with N. Höflich [19].

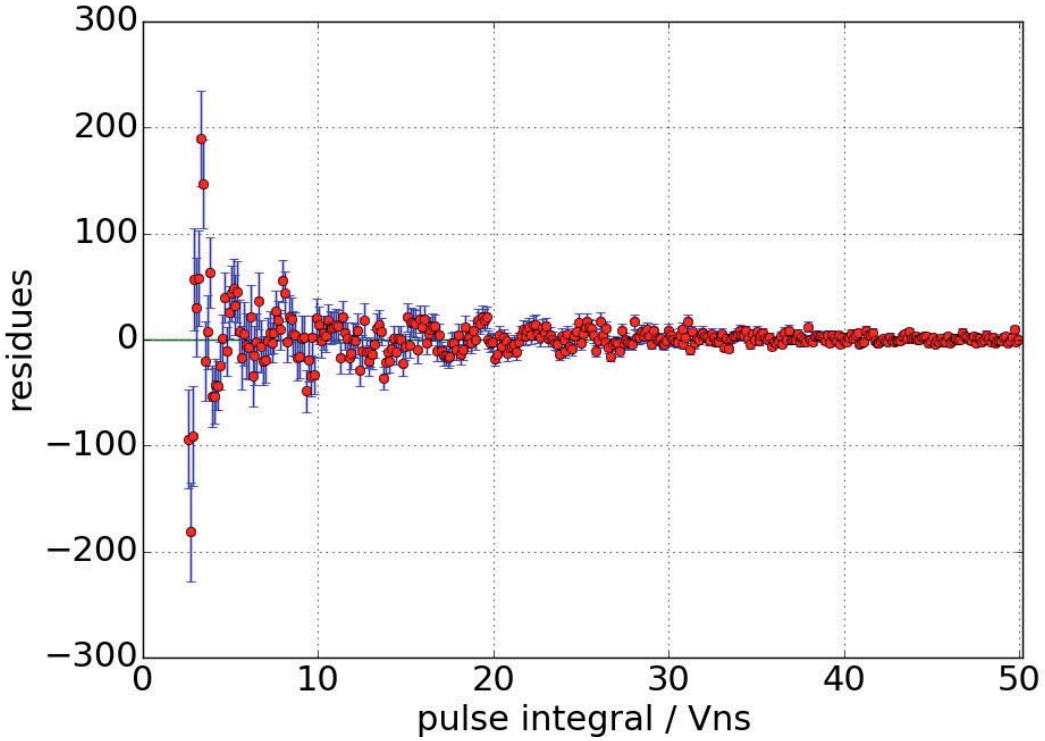

Figure 4.6: The residuum of the plot 4.5. The residuum shows an oscillation, which means that there is a small offset between the fit and the data. With another number of Gaussian functions, the oscillation is still there and can not be removed. This figure is created together with N. Höflich [19].

The *gain* is calculated to (figure 4.5):

$$gain = (3.117 \pm 0.012)\,\text{nVs}. \tag{4.6}$$

For comparison, the calculated *gain* in the other measurement for the same pixel, also done with the FACT-function, was determined to

$$gain_2 = (3.128 \pm 0.013)\,\text{nVs}. \tag{4.7}$$

The values of the *gain* matches within the errors.
The calculated crosstalk-probability p_{xt} is determined to

$$p_{\text{xt}} = 0.5144 \pm 0.0059. \tag{4.8}$$

For comparison, the calculated p_{xt} in the other measurement for the same pixel, also done with the FACT-function, was determined to

$$p_{\text{xt}} = 0.5173 \pm 0.0063. \tag{4.9}$$

The crosstalk-probability matches within the errors in both measurements, too.
The higher p.e.-peaks does not fit very well to the FACT-fit (figure 4.5), they are not as high as the real data. Furthermore the residuum (figure 4.6) shows an oscillation. This means that the distance between the peaks is calculated too small. For this reasons, the FACT-function is fitted again, but only for the first five peaks.

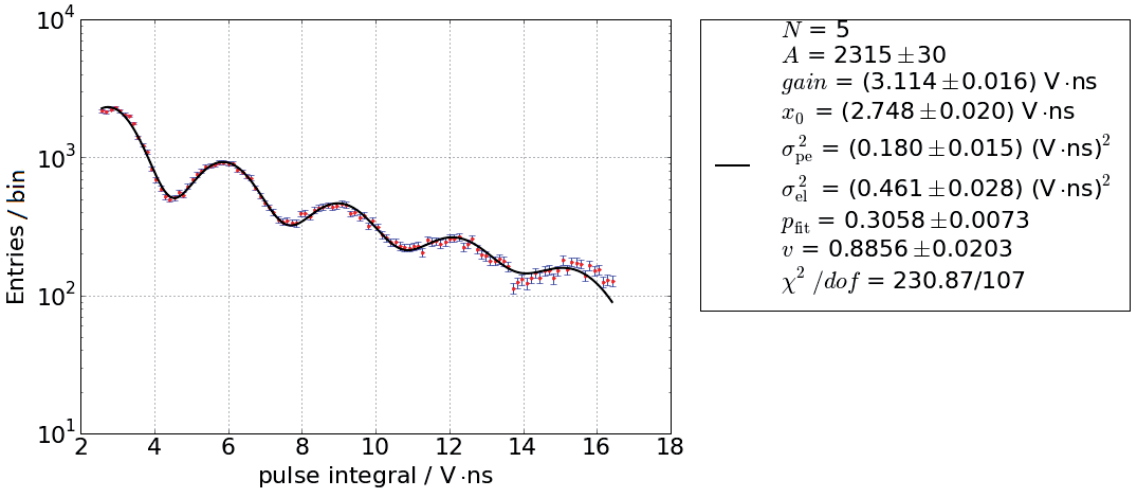

Figure 4.7: FACT-fit at the first five fingers of the histogram of the integrated SiPM-signals of the middle pixel from the FAMOUS telescope camera. The fit describes the data well for the first four fingers, the last one differs at the end, because the Fit is made for five fingers, but the data is influenced by the sixth finger. The parameters can be found at the right side of the figure. This figure is created together with N. Höflich [19].

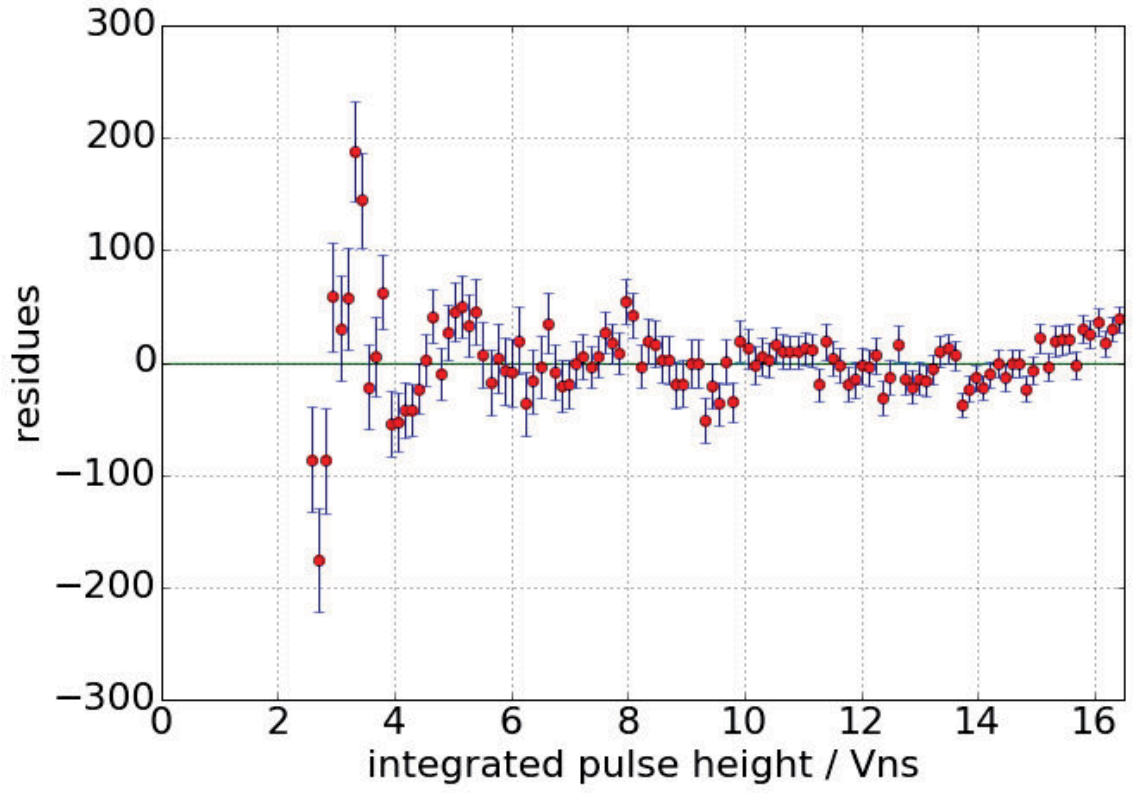

Figure 4.8: Residuum of the plot in figure 4.7. The residuum shows a small oscillation, but most of the residuum fluctuats about zero. The difference between the data and the fit at the end of the residuum results from the number of fitted Gaussian functions. The fit considers only five peaks, while the data includes more peaks and the sixth peak overlaps with the fifth. This figure is created together with N. Höflich [19].

With the fit over 5 peaks, the *gain* is calculated to

$$gain = (3.114 \pm 0.016)\,\mathrm{nVs}. \tag{4.10}$$

The calculated *gain* is smaller than before with a fit over 16 peaks, but the values agree within the uncertainty limits. The crosstalk-probability of
$p_{\mathrm{xt}} = 0.517 \pm 0.012$ matches with the other probabilities, too. Here should be said, that the calculated crosstalk-probability is very high. The expected crosstalk-probability is about $30 - 35\,\%$. An explanation would be that some cells fire at the same time and the individual signals are seen as one signal, for example two 1-p.e. signals appear as one 2-p.e. signal.
All in all, the *gain* and the crosstalk-probability of the SiPMs can be determined with an oscilloscope and the programs for the evaluation of a finger-spectrum are prepared for the next measurements with the TARGET7-module.

Comparison of the SiPMs in the FAMOUS Telescope

For the following measurements it is useful to check, if the SiPMs in the FAMOUS telescope have similar characteristics.

Gain

The calculated *gain* of both measurements agrees within the uncertainties for all used pixels, except of the pixels 29, 38 and 47. The minimal calculated *gain* lies at $(3.064 \pm 0.018)\,\mathrm{nVs}$, the maximal *gain* at $(3.273 \pm 0.013)\,\mathrm{nVs}$. The difference between these values is relatively high for the same models of SiPMs. Otherwise, the maximal *gain* is measured from the blind pixel, so it is not an important pixel for a measurement. The *gain*s of the other SiPMs correspond better (figure 4.9).

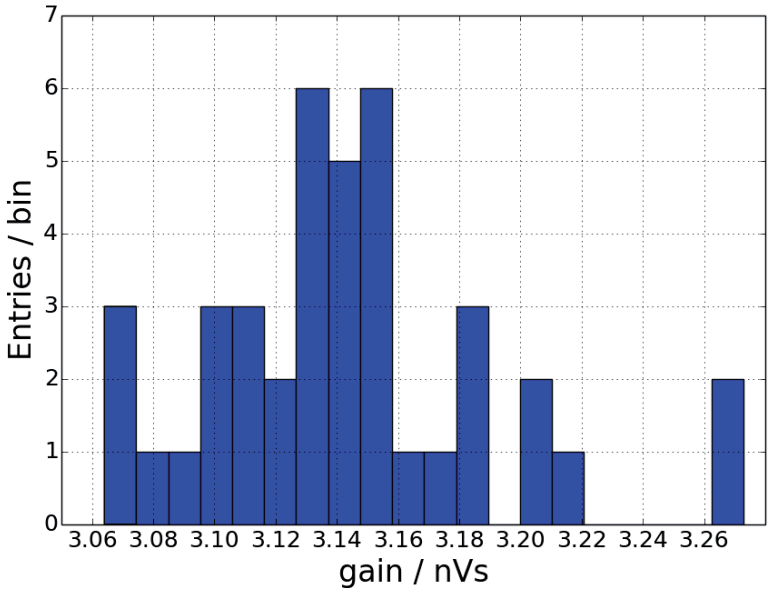

Figure 4.9: Histogram of the calculated *gain*s of the pixels in the FAMOUS telescope. The *gain* is dispersed around 3.14 nVs. The *gain*s have a maximal distance of 4.24 % to the cluster point.

As it is shown in the histogram (figure 4.9), most of the calculated *gain*s are dispersed around 3.134 nVs. The differences between the *gain*s are relatively small, about 1.27 %. The only outlier, the blind pixel, is not included in the measurement, so that it is less important than the difference between the other pixels. The differences are probably correlated with the differences of the overvoltage. The overvoltage fluctuates around 1.4 V for all pixel, with little uncertainties. Regarding the uncertainties of the overvoltage and of the components of the SiPMs, the results fulfil the expectations.

Crosstalk Probability

To check the resemblance of the used pixels, the calculated crosstalk probability is shown in a histogram and analysed, too. Except of pixel 30 and pixel 38, the values for the crosstalk probability of both measurements agree within the uncertainties.

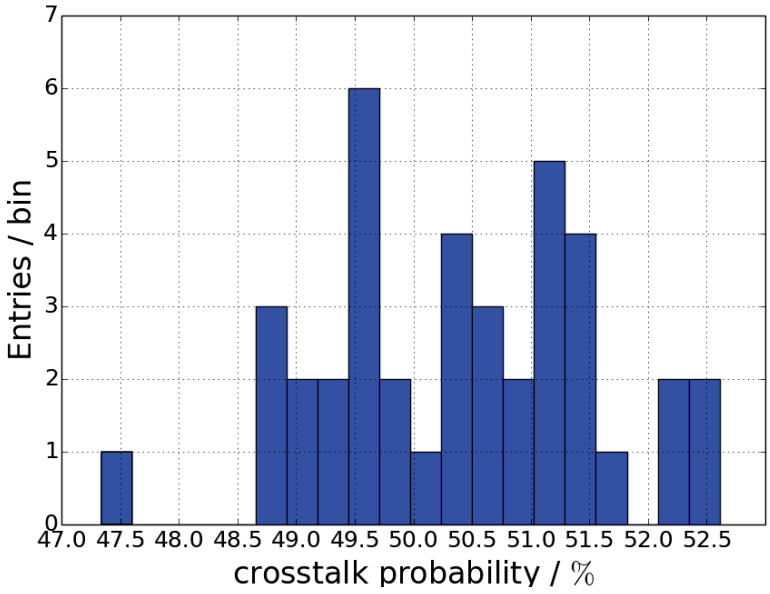

Figure 4.10: Histogram of the calculated crosstalk probabilities of the pixels in the FAMOUS telescope. The crosstalk probability is dispersed around 50.4 %.

The lowest crosstalk probability lies at (47.34 ± 0.58) %, the highest at (52.61 ± 0.60) %. The crosstalk probability fluctuates about 2 % around the mean of 50.4 %. As a result can be said, that the crosstalk probabilities are comparable, but not as equal to the expectation. This may be correlated to the fact, that the calculated crosstalk probability is higher than expected, like it was said before.

4.2 Measurement with the TARGET 7

This chapter deals with the measurements with the FAMOUS telescope and the TARGET7-module as the read-out board. The TARGET7-module is used during night measurements outside, in front of the lecture hall of physics of the RWTH Aachen, Germany. Later, the TARGET7-module is also used for dark-measurements in the hall of physics of the RWTH Aachen, Germany.

4.2.1 Dark-measurement

The SiPM-signals must be analysed, to make quantitative statements about the measurements with the FAMOUS telescope, using the TARGET7-module as the read-out board. The SiPM-signals looks different when they are read out with the TARGET7-module than with the oscilloscope, so that the results of chapter 4.1 can not be used.
Firstly, the SiPM-signal has to be identified. Later, there will be tried to find the *gain* of the SiPM-signals.

4.2.1.1 Set-up

The set-up for the dark-measurement is similar to the set up for the measurement to find the right trigger delay of the TARGET7 (chapter 3.3.2). For the dark-measurements, the pulse generator is connected only to the external trigger input of the TARGET7-module and not connected to the patch-board. Instead, 16 pixels (figure 4.14) of the FAMOUS-telescope are connected to the TARGET7-module. Furthermore, the FAMOUS telescope is activated as described in chapter 4.1.1 with an overvoltage of 1.4 V.
For the dark-measurement the external trigger of the TARGET7-module is used. The Vped of the TARGET is set to 1500 DAC − counts and the trigger delay is set to 424 ns.
The frequency of the pulse generator for causing the read-out is set to 30 Hz. For the finger-spectrum 257 measurements are taken, each over 20 s.

4.2.1.2 Finger-spectrum

To determine the *gain* of the SIPMs, there is tried to make a finger-spectrum. Firstly, the SiPM-signal has to be identified (figure 4.11). The SiPM-signal looks different than with the oscilloscope, so that the integration method has to be changed. The SiPM-signal consist of two parts, the high positive part and then a lower negative part.

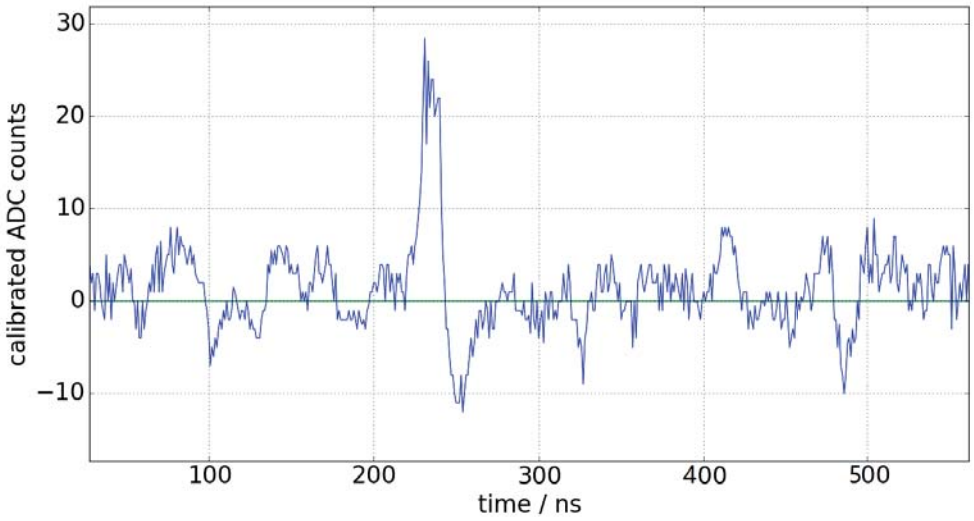

Figure 4.11: SiPM-signal taken with the TARGET7-module, zoomed into a calibrated trace. The SiPM-signal taken with the Oscilloscope looks different than when it is taken with the TARGET7-module. The bandpass-filter, which is implemented in the TARGET7-module, works as a differentiator and changes the form of the SiPM-signal. The calibration has been done by N. Höflich.

Firstly, all traces are calibrated by N. Höflich [19]. After the calibration, the peak-finder is used to find all positive peaks with a minimal height of 13 ADC − counts and a minimal distance of 200 ns between two peaks.
The integration over the SiPM-signal is changed to 7 ns before the peak and 8 ns after the peak. The filter with the slope to filter the characteristic electric noise of the laboratory is removed, because the slope of the SiPM-signal and the slope of the noise are the same.
Figure 4.12 shows the resulting histogram with 1024 bins. The histogram shows no characteristic fingers, with the consequence that the *gain* cannot be determined with the histogram. Reasons for the missing fingers could be the electric noise, which can reach the height of the one p.e.-signal, as well as the characteristic electric noise of the location. Maybe, the gain of the pre-amplifier is too low. The fingers could not be produced with other integration methods.

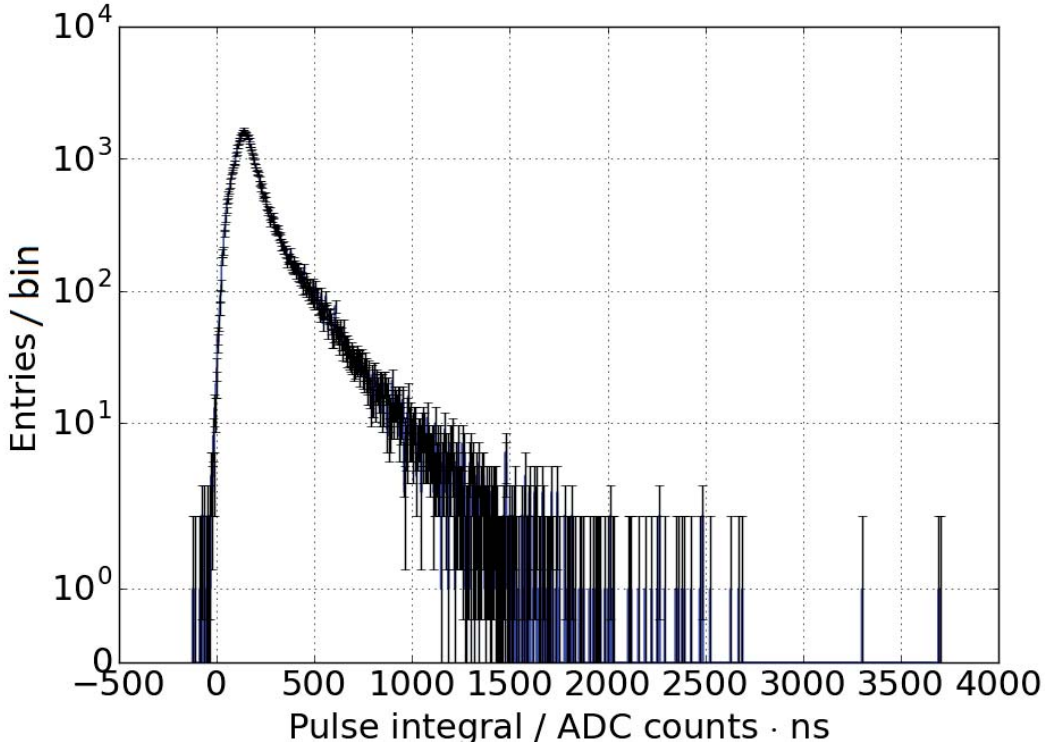

Figure 4.12: Histogram of the integrated SiPM-signals. The characteristic fingers of the SiPMs in the logarithmic display can not be seen. This figure is created together with N. Höflich [19].

4.2.1.3 Estimation of the 1 p.e. signal

As the *gain* could not be determined with the histogram of the integrated values, another method must be found for the estimation of the *gain*. For this reason single SiPM-signals are searched in the traces of the dark-measurements manually. The comparison of the height of the SiPM-signals and the integral over those allows to estimate the height and the integral of the 1-p.e.-signal.
Because of the height electric noise and the fluctuation of the integrals, the estimation of the integral of the 1-p.e.-signal is very inaccurate.
The calculation of the integral over the 1-p.e.-signal delivers the result:

$$I_{1\,\mathrm{p.e.}} \approx 120\,\mathrm{ADCcounts} \cdot \mathrm{ns}. \tag{4.11}$$

The result is reviewed with another method. With the knowledge of the crosstalk-probability of about 50 %, the fingers of the histogram should have half of the height of the finger before. For that reason, the histogram is checked if the number of entries halves itself after 100 ADCcounts · ns. In a good approximation, this statement is correct. As a consequence, the result can be taken as a rough estimation for the *gain*, even if the method is very inaccurate. More details can looked up in the Bachelor-thesis of N. Höflich [19].

4.2.2 Measurement of Cherenkov-light candidates

The TARGET7-module shall be used as the read-out-board for the FAMOUS telescope. For this reason, it has to be tested if it is possible to measure air showers. In order to prove it, the FAMOUS telescope was taken outside at night. The measurement was done in the night of the 24th to the 25th of August, 2016. The measurement for the calibration started at 23:44:42 o'clock. The real measurement started at 01:15:30 o'clock and ended at 02:40:03 o'clock. After it, there was done more calibration measurements. During the measurements, the FAMOUS telescope was oriented at the west and as vertical as possible (figure 4.13).
The FAMOUS telescope is constructed to measure fluorescence light, but this is very difficult in Aachen, because of the bright night sky. Accordingly, it was searched for Cherenkov shower instead of fluorescence light.

4.2.2.1 Set-up

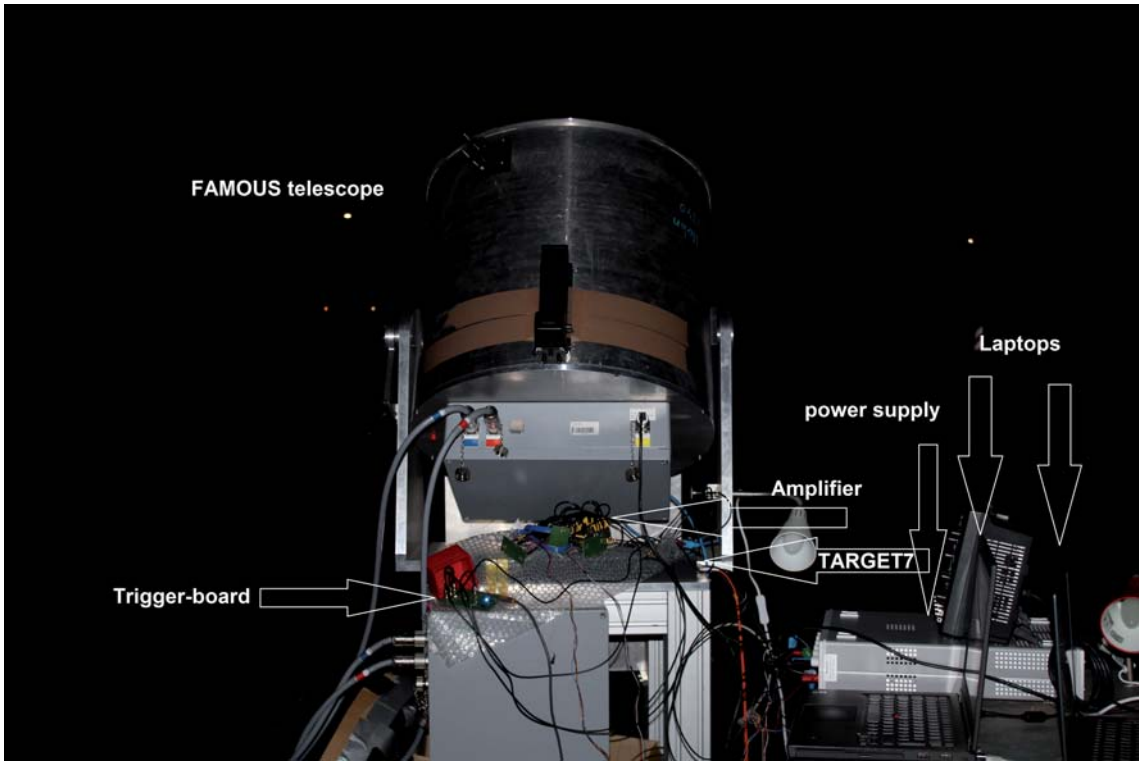

Figure 4.13: Set-up of the outside measurement with the FAMOUS telescope and the TARGET7-module.

As a power source during the outside measurement a petrol-operated generator. An extension cable and multi-plugs made it possible to connect all electric devices to the power source.
For the measurement two laptops have been used. One laptop is connected to the FAMOUS telescope via LAN and to the trigger-boards via USB. The trigger board is built by J. Schumacher. It has four ports, three input ports and one output port. Each inputport is connected to a pixel of the FAMOUS telescope via an amplifier (built by J. Schumacher). These three pixels are used as the trigger-pixels (figure 4.14). The trigger-board waits until one signal is higher than the threshold. If there is such a signal, the trigger-board gives a signal out of the output port. The threshold

can be set using the connected laptop. The output signal is connected to the external trigger input of the TARGET7-module. The TARGET7-module is connected to the power supply and to the second laptop through a switch. Furthermore, patch-board connects the TARGET7-module tp 16 pixels of the FAMOUS telescope.

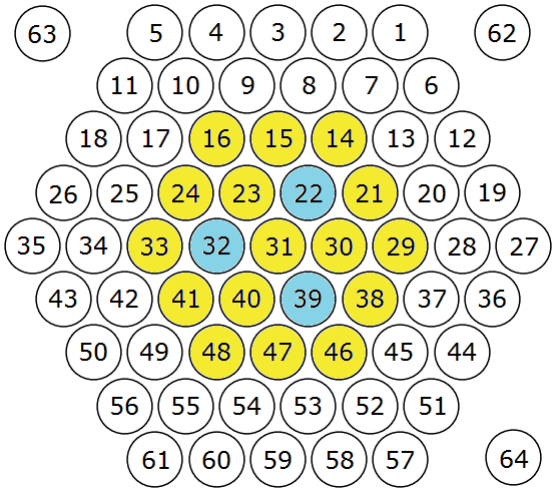

Figure 4.14: Layout of the camera in FAMOUS. The yellow marked pixels are connected to the TARGET7-module, the blue pixels are used as the trigger-pixels [19].

4.2.2.2 Data acquisition

The following settings are used during the measurement outside:
The overvoltage of the SiPMs are set to 1 V for measuring higher p.e.-signals and because of the bright environment.
The external trigger of the TARGET7-module is used, because the self-trigger does not work yet.
A trigger delay of 424 ns is used, to see the signals in the trace, which caused the read out.
The threshold for the trigger board is set at 0.93 V, which causes an average frequency of 0.44 Hz of triggering. 8 successfully measurements have been done, each with a length of 5 min.
The trigger pixels are not chosen randomly. Each trigger pixel is surrounded by pixels, connected to the TARGET7-module (figure 4.14). If cherenkov light hits the trigger pixel, the probability of hitting more pixels next to the trigger pixel is very high. If the trigger pixel causes a read out, coincidental events next to the trigger pixel should be noticed.

4.2.2.3 Evaluation

To start the evaluation, the traces are inspected, whether high signals can be seen at the first look. Indeed, it is possible to find some high SiPM-signals in some traces, like it is shown in figure 4.15. These traces are all already corrected by N. Höflich. The SiPM-signal is about 70 times higher, than the signal in figure 4.11. This could be an evidence, that the signal could be caused by Cherenkov-light. To support this suspicion, other channels must be analysed in a similar time frame.

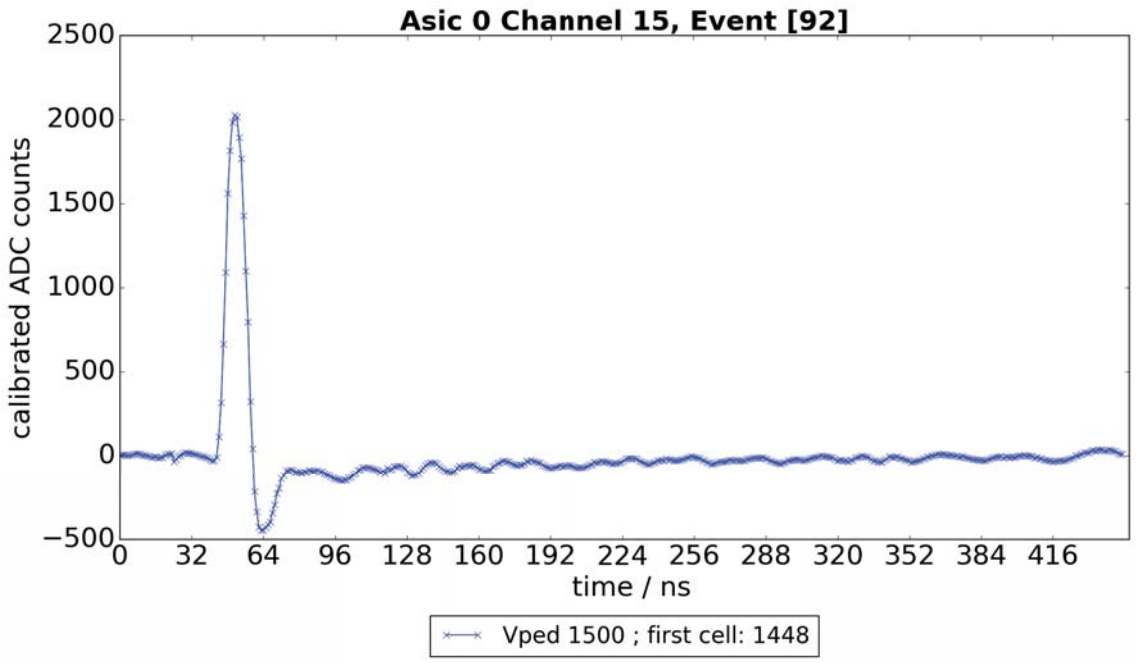

Figure 4.15: Trace taken during the night measurement outside with the FAMOUS-telescope and the TARGET7-module as the read-out-board. A high SiPM-signal can be seen in this event. This figure is created together with N. Höflich [19].

A look at the close channels shows some interesting circumstances. Figure 4.16 shows the pixel next to the pixel considered figure 4.15 and the SiPM-signal does not look like a normal SiPM-signal. Two phenomenons stands out: The SiPM-signal seems to be cut off at the top and the negative dip of the signal is shifted to a later time. The first thing is curious, because the SiPM-signal is only about 2500 ADC − counts high, so in the raw data it would have a height of about 3500 ADC − counts. Theoretically, it should be possible to measure up to 4096 ADC − counts. This could probably mean, that the last 500 ADC − counts are not able to measure because of the saturation of the pre-amplifiers. This is only one possibility to explain the cut off and this was not examined anymore.
The second conspicuousness could be caused by two different things. Firstly, by the shower itself. It could be, that the shower is about 160 ns long, but this can not bee seen due to the saturation. This would mean, that the dip appears at the right position. Another possibility is, that the dip is shifted by a delay caused by the electronics, that it has a problem with the saturation. When a Signal causes a saturation, other channels are affected by curiosities like a dip down before the signal arrives (figure 5.6 in the appendix). These may very likely be electronic problems which appear following the existence of high signals.

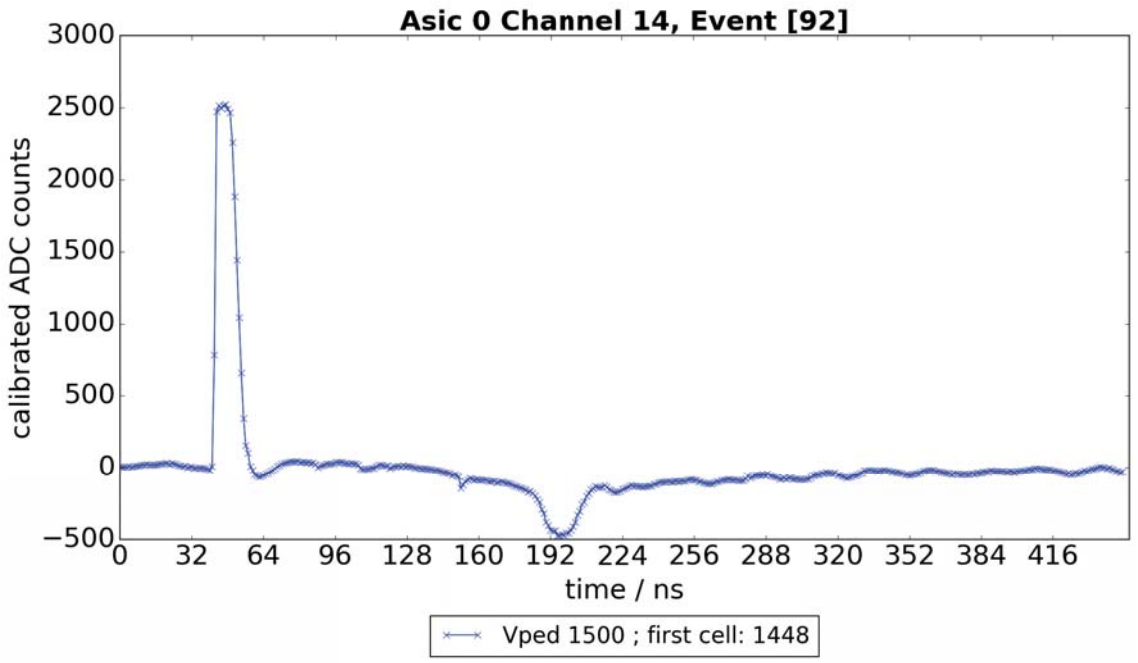

Figure 4.16: Trace taken during the night measurement outside with the FAMOUS-telescope and the TARGET7-module as the read-out-board. The SiPM-signal has a hight of about 2500 ADCcounts, in the raw data is would be about 1000 ADCcounts more. It is interesting that the signal is cut of at the top, without reaching the maximum of 4096 ADCcounts. Furthermore, the negative dip is shifted to a later time. Probable causes are the electronics affected by the saturation or by the size of the shower itself. More details in the text. This figure is created together with N. Höflich [19].

The next step in the data analizing process is to search for SiPM-signals caused by photons which hit the detector at approximately the same time. Therefore are searched for peaks with a minimal peak height of $200\,\mathrm{ADC-counts}$. For these peaks, the different channels are compared in the same event, if there can be found more signals. If there are at least two signals, the integration over the peaks starts (same integration method as in chapter 4.2.1.2). For calculating the number of photons, the results from the dark-measurement can be used. Therefore it is important to consider the different overvoltage. The overvoltage changes the integration in a linear way, so that the conversion is very easy. The integration value over one signal is

$$I_{1\,\mathrm{p.e.}} = 120\,\mathrm{ADCcounts}\cdot\mathrm{ns}\cdot\frac{1\,\mathrm{V}}{1.4\,\mathrm{V}} \approx 85.7\,\mathrm{ADCcounts}\cdot\mathrm{ns}. \tag{4.12}$$

The search for SiPM-signals in more than one channel results in 17 events. An example is shown in figure 4.17.

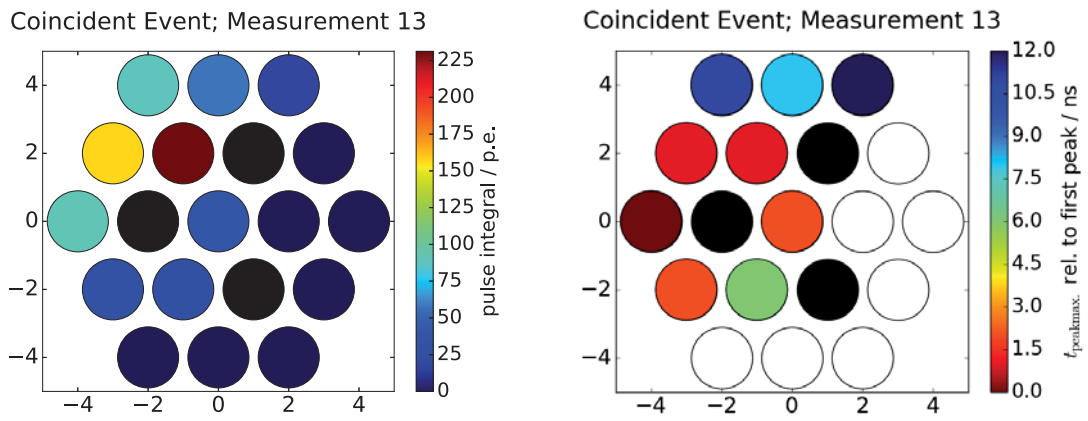

Figure 4.17: The left figure: Layout of the 19 pixels which are connected during the night measurement. The black marked pixels are used for the trigger. The scale at the side shows how many photons hit the pixels. For the red pixel it is only the minimal number of photons, because of the cut off at the top of the signal. If no signal with a minimal peak of 200 ADC − counts was detected, there was no integration over the signal and it was approximated as 0.
The right figure: Layout for the same measurement as the left figure. Here is shown the relative time difference between the first signal and the other signals in ns. The time-scale can be seen at the right side of the figure. The detection time of the first signal is set to 0 ns. The white pixels had no signal. The layouts are done by N.Höflich [19].

Because of the high number of pixels which registered a high number of photons in a very short time difference, the measured signal represents most likely the detection of Cherenkov light. It is very improbable that the signals are caused by the brightness of the sky.
In conclusion it can be said that in 40 min of measurement at night, 17 events with coincidences in at least three pixels were found, all likely caused by Cherenkov light. With this measurements it is shown that it is possible to measure Cherenkov light with the TARGET7-module. For better estimation of the number of photons, the calculation of the 1 p.e. − signal should be improved. Furthermore, it could be a possibility to change the Vped for the measurement. This could prevent the cut off of the SiPM-signal. On the other hand, the Vped should not be set too small, so that the negative dip can be measured. Otherwise it is difficult to say, if the measured signal is really a SiPM-signal. The choice of an overvoltage of 1 V has shown good results.

5. Summary and Outlook

In this Bachelor-thesis, the work with the FAMOUS telescope and the TARGET7-module were presented.
At first, 20 of the 64 pixels were used for dark measurements with the oscilloscope to create finger spectra. The recorded data was analysed for all pixels, so that it was possible to calculate characteristics of the SiPMs like the *gain* or the crosstalk probability. Furthermore, the *gain* and the crosstalk probability of each pixel were compared.
Moreover, the TARGET7-module was employed. The different trigger types were analysed and used. Because the results of the measurements with the oscilloscope cannot be used for measurements with the TAREGT7-module, the hardsync trigger was used for dark measurements. The determination of the *gain* by using the finger spectra failed, but it was possible to estimate the *gain* with other methods. Furthermore, the hardsync trigger was used during the first night measurements outside with the TARGET7-module as the read out board for the FAMOUS telescope. Signals, which are caused likely by Cherenkov light, were recorded successfully during the night measurements.
The self trigger of the TARGET7-module was understood and the first steps for the activation of the self trigger are done. Successes and problems during the commissioning of the self-trigger were presented and discussed.
In future studies, all pixels of the FAMOUS telescope should be used for measurements, this is already in work. Furthermore, new dark measurements with the TARGET7-module should be done for a better calculation of the *gain*. Moreover, the next steps for self trigger should be done to use it in future measurements outside.

Acknowledgements

Zu aller erst bedanke ich mich bei Prof. Dr. Thomas Bretz und Prof. Dr. Thomas Hebbeker, die mir die Möglichkeit gegeben haben diese Bachelorarbeit zu erarbeiten und daran zu wachsen. Es war eine großartige Erfahrung am Projekt FAMOUS mitarbeiten zu dürfen und dafür bedanke ich mich ganz herzlich.

Ein ganz großer Dank geht an meinen Betreuer Johannes Schumacher. Er war jederzeit hilfsbereit, hat sich jegliche Probleme angehört und zur Lösung dieser beigetragen. Nicht nur, dass er mir eine ganze Menge beigebracht hat, er hat mit seinen Beiträgen die Messungen nachts ermöglicht und diese dann auch noch aktiv unterstützt. Des Weiteren hat er diese Arbeit inhaltlich und sprachlich stark verbessert, für all das ein ganz großes Dankeschön.

Die nächste Person, der ich danken möchte, ist Nina Höflich, mit der weite Teile dieser Bachelorarbeit zusammen erarbeitet wurden. Vielen Dank, dass wir zusammen sowohl messen, als auch auswerten konnten. Nina war ebenfalls jederzeit bereit an einer Lösung von jeglichen Problemen mitzuarbeiten und eine Lösung zu finden.

Der nächste Dank geht an jegliche Doktoranten, Masteranten und Bacheloranten im Institut III A und B, die jederzeit ansprechbar waren und stets hilfreiche Hinweise gaben.

Ein großer Dank geht auch an alle Freunde und Bekannte, die diese Arbeit Korrektur gelesen und das sprachliche Niveau nochmals angehoben haben. Dafür ein herzliches Dankeschön, von meiner Seite aus und von der Seite aller Leser.

Letztlich noch der Dank an meine Familie und Freunde, die jederzeit einem zur Seite standen und sowohl bei kleinen, als auch bei großen Dingen geholfen haben, die einem das Leben während der Arbeit erleichtert haben.

Literatur

1. <www.Auger.org>.
2. Particle Data Group. *Cosmic Rays* <http://pdg.lbl.gov/2015/reviews/rpp2015-rev-cosmic-rays.pdf> (2015).
3. John Hewitt. Cosmic rays could power subsurface life in the universe (2015).
4. <www.ung.si>.
5. Prof. Dr. Lutz Feld. *Skript zur Vorlesung der Experimentalphysik Vb - Teilchen- und Astrophysik WS 2015/16*
6. The Pierre Auger Cosmic Ray Observatory. *Elsevier* (2015).
7. Blümer, J., Engel, R. & Hörandel, J. R. Cosmic rays from the knee to the highest energies. *Progress in Particle and Nuclear Physics* **63,** 293–338 (Oct. 2009).
8. Hans Micheal Eichler. *Characterisation studies on the optics of the prototype fluorescence telescope FAMOUS* MA thesis (RWTH Aachen, 2014). <https://web.physik.rwth-aachen.de/~hebbeker/theses/eichler_master.pdf>.
9. <wwwo.physik.rwth-aachen.de>.
10. Prof. Dr. Wolfgang Demtröder. *Laserspektroskopie - Grundlagen und Techniken* (1999).
11. Aull, Brian F and Loomis, Andrew H and Young, Douglas J and Heinrichs, Richard M and Felton, Bradley J and Daniels, Peter J and Landers, Deborah J. Geiger-mode avalanche photodiodes for three-dimensional imaging. *Lincoln Laboratory Journal* **13,** 335–349 (2002).
12. Johannes Schumacher. *Characterization Studies of Silicon Photomultipliers: Noise and Relative Photon Detection Efficiency* Bachelor Thesis (III. Phys. Inst. A, RWTH Aachen University, Germany, 2011).
13. Mazin, D., Bangale, P., Sitarek, J., Cortina, J., Fink, D., Hose, J., Illa, J. M., Lorenz, E., Martínez, M., Menzel, U., Mirzoyan, R. & Teshima, M. Towards SiPM camera for current and future generations of Cherenkov telescopes. *ArXiv e-prints.* arXiv: 1410.5070 [astro-ph.IM] (2014).
14. Niggemann, T., Assis, P., Brogueira, P., Bueno, A., Eichler, H. M., Ferreira, M., Hebbeker, T., Lauscher, M., Mendes, L., Middendorf, L., Navas, S., Peters, C., Pimenta, M., Ruiz, A., Schumacher, J. & Stephan, M. Status of the Silicon Photomultiplier Telescope FAMOUS for the Fluorescence Detection of UHECRs. *ArXiv e-prints.* arXiv: 1502.00792 [astro-ph.IM] (Feb. 2015).
15. Hamamatsu MPPCC - Technical Information.

16. Lars Steffen Weinstock. *Development of front-end electronics for detectors with SiPM readout* MA thesis (Physics Institute III B, RWTH Aachen University, Germany, 2014).

17. Tim Niggemann. *THE SILICON PHOTOMULTIPLIER TELESCOPE FAMOUS FOR THE DETECTION OF FLUORESCENCE LIGHT* Doctor thesis (Institut III A, RWTH Aachen, To be published November 2016).

18. Hamamatsu - News 2008.

19. Nina Höflich. *Implementation and calibration of the TARGET data acquisition system for FAMOUS* Bachelor Thesis (III. Physikalischen Institut A, RWTH Aachen University, Germany, To be published 2016).

20. Erik Ganster. *Test des TARGET-7-Datenerfassungsmoduls für das IceACT Luft-Cherenkov-Teleskop* Bachelor Thesis (III. Physikalischen Institut B, RWTH Aachen University, Germany, 2016).

21. <www.cta-observatory.org>.

22. Tibaldo, L., Vandenbroucke, J. A., Albert, A. M., Funk, S., Kawashima, T., Kraus, M., Okumura, A., Sapozhnikov, L., Tajima, H., Varner, G. S., Wu, T., Zink, A. & CTA consortium, f. t. TARGET: toward a solution for the readout electronics of the Cherenkov Telescope Array. *ArXiv e-prints*. arXiv: 1508.06296 [astro-ph.IM] (2015).

23. <http://www.spacetelescope.org/projects/fits_liberator/>.

24. Dr. Adrian Zink. *Personal e-mail communication* 2016.

25. Christoph Günther. *Temperature Dependence of the SiPMs and the front-end Electronicsfor AugerPrime* Bachelor Thesis (III. Physikalischen Institut A, RWTH Aachen University, Germany, To be published 2016).

26. Marcos Duarte. <https://github.com>.

27. Biland, A., Bretz, T., Buß, J., Commichau, V., Djambazov, L., Dorner, D., Einecke, S., Eisenacher, D., Freiwald, J., Grimm, O., von Gunten, H., Haller, C., Hempfling, C., Hildebrand, D., Hughes, G., Horisberger, U., Knoetig, M. L., Krähenbühl, T., Lustermann, W., Lyard, E., Mannheim, K., Meier, K., Mueller, S., Neise, D., Overkemping, A.-K., Paravac, A., Pauss, F., Rhode, W., Röser, U., Stucki, J.-P., Steinbring, T., Temme, F., Thaele, J., Vogler, P., Walter, R. & Weitzel, Q. Calibration and performance of the photon sensor response of FACT the first G-APD Cherenkov telescope. *Journal of Instrumentation* **9,** P10012 (Oct. 2014).

Appendix

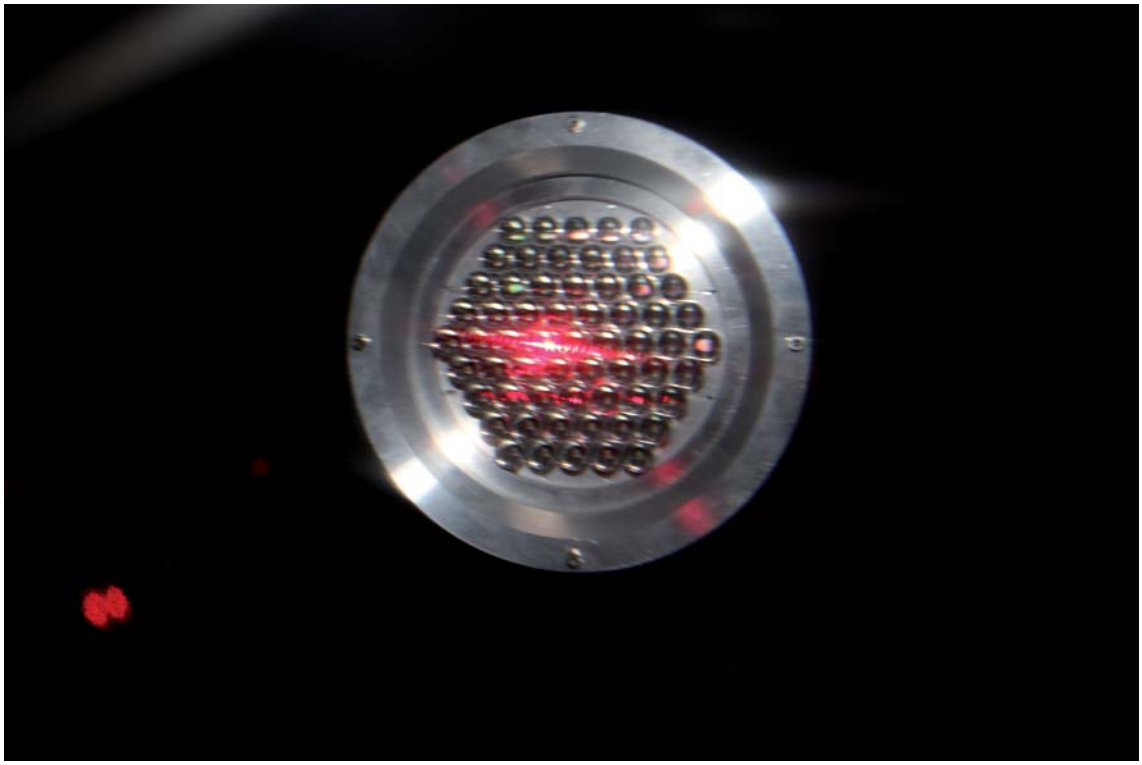

Figure 5.1: The 61-pixel camera of the FAMOUS telescope. Here, a red laser-pointer to focus the light at the individual pixels. Because of the reflection and the Fresnel lens, it can not be seen in this picture, that the really is focused on only one pixel. On the other hand, the camera can be seen well. The picture was taken by Benjamin Pestka

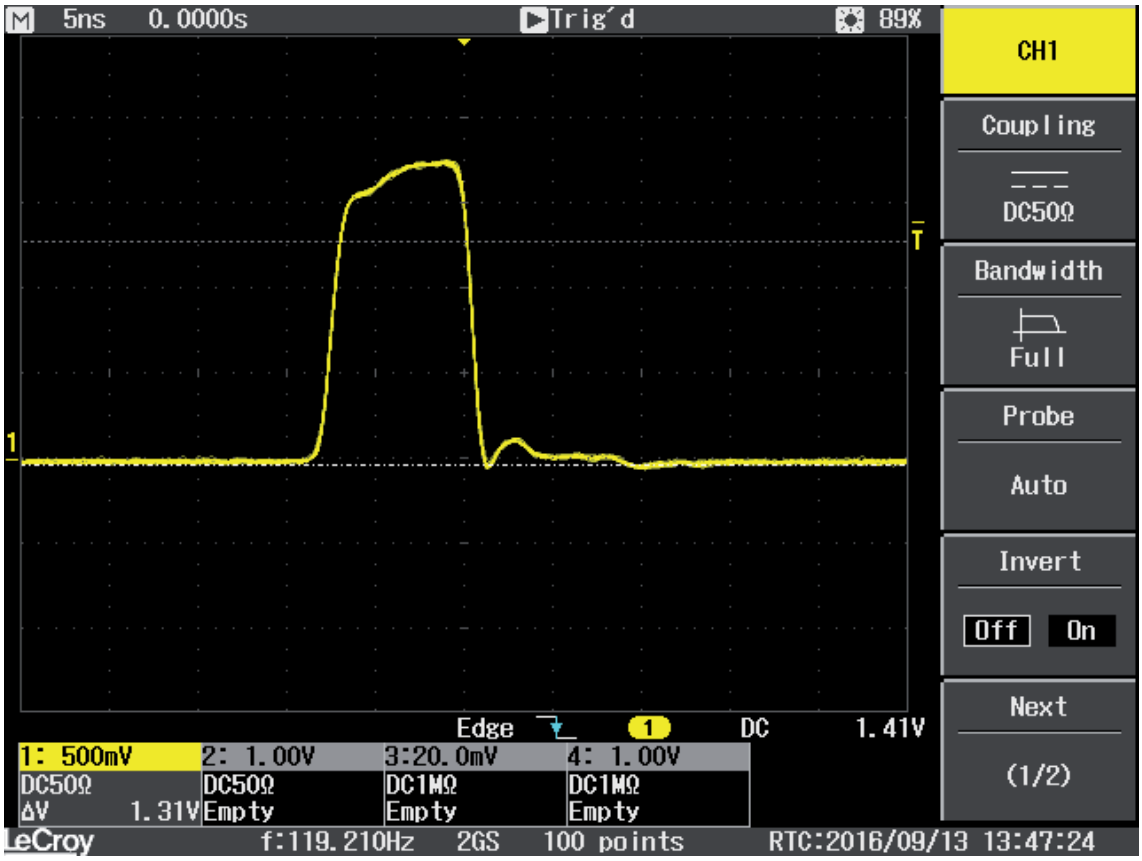

Figure 5.2: Signal of the trigger output of the TARGET7 during a measurement with the hardsync trigger. Screenshot taken with the Lecroy WJ354A oscilloscope. The x-axis represents the time, each box stands for 5 ns. The y-axis represents the measured voltage, each box stands for 500 mV.

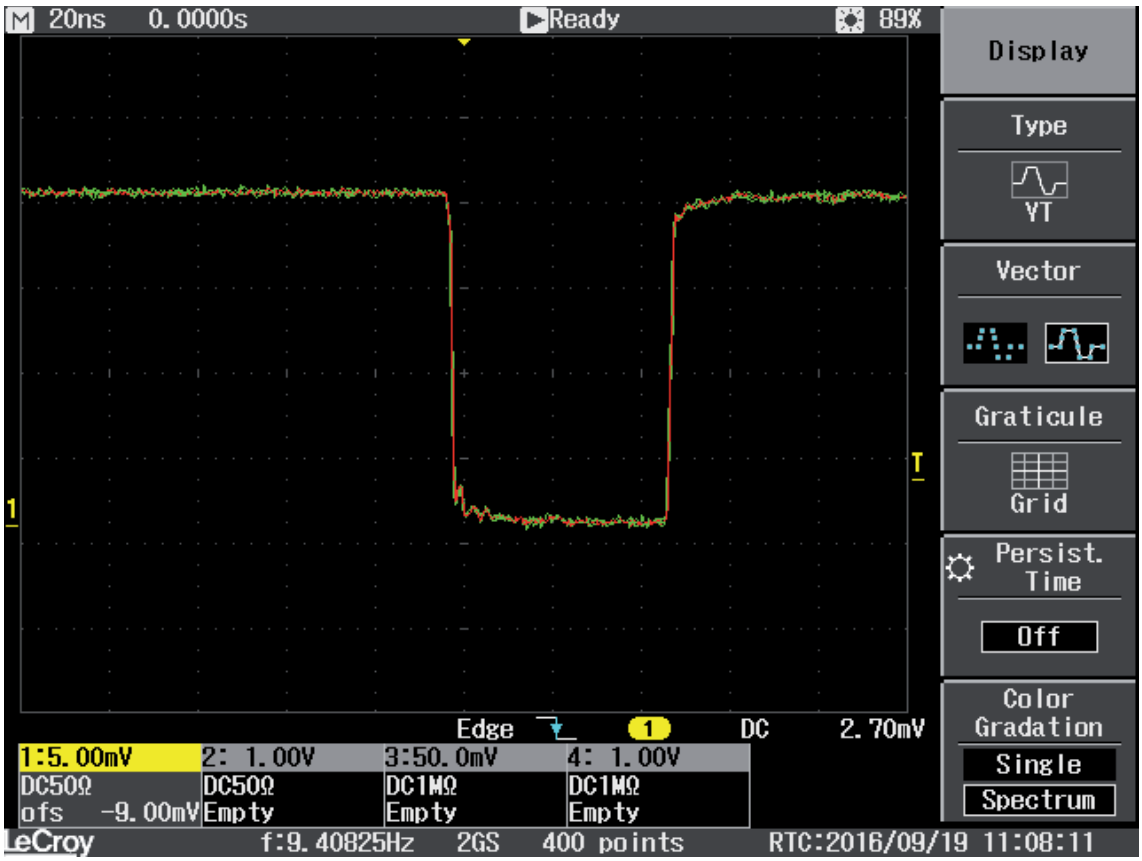

Figure 5.3: The inverted signal of the pulse generator for the measurement of the trigger delay with the external trigger of the TARGET7-module. Screenshot taken with the Lecroy WJ354A oscilloscope.
The x-axis represents the time, each box stands for 20 ns. The y-axis represents the measured voltage, each box stands for 5 mV.

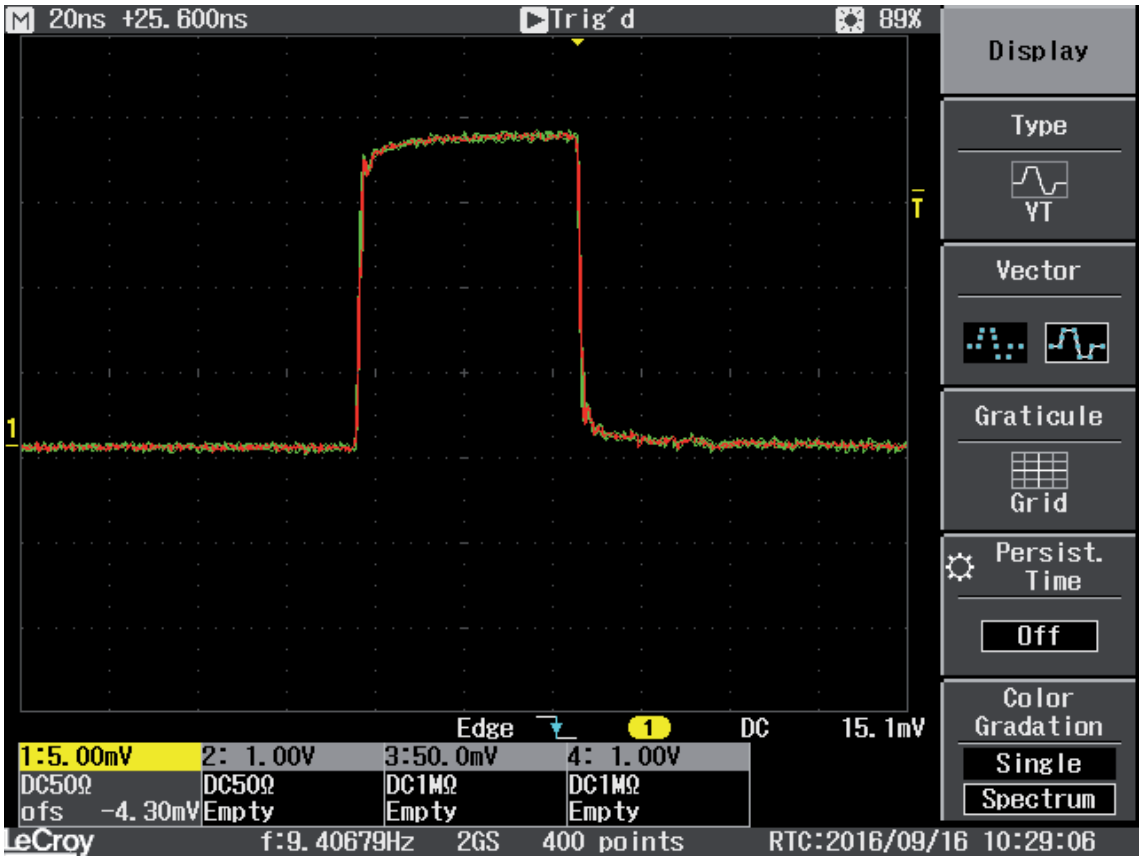

Figure 5.4: The signal of the pulse generator for the test of the self-trigger of the TARGET7-module. Screenshot taken with the Lecroy WJ354A oscilloscope.
The x-axis represents the time, each box stands for 20 ns. The y-axis represents the measured voltage, each box stands for 5 mV.

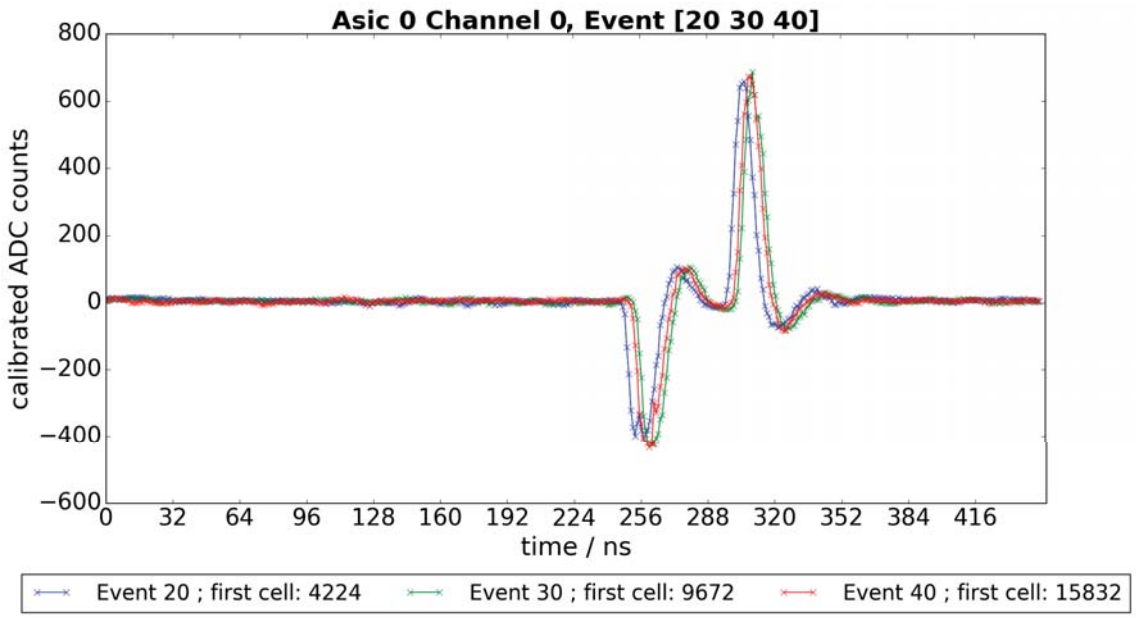

Figure 5.5: Here can be seen a trace, measured with the TARGET-module, triggered with the external trigger. The signal input on channel 0 is a inverted square-wave signal (figure 5.3) and to see the signal in the trace, here is used a trigger delay of 585 ns. By comparison of the input signal and the measured signal, there can be seen that the bandpass-filter of the TARGET7-module seems to work as a differentiator.

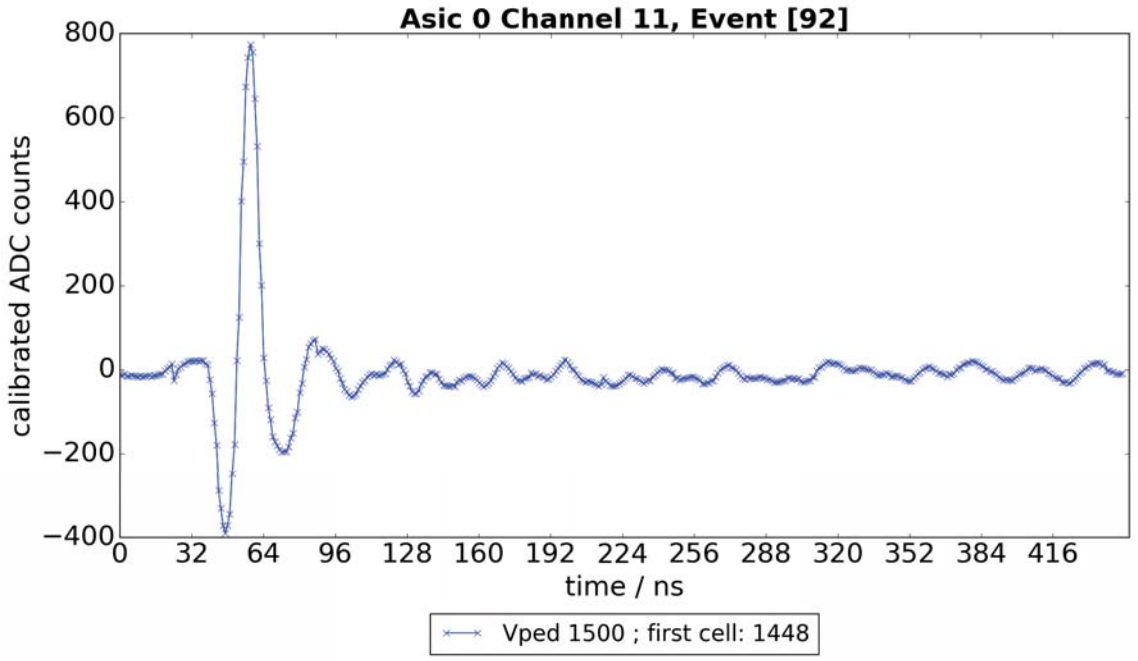

Figure 5.6: Trace taken during the night measurement outside with the FAMOUS-telescope and the TARGET7-module as the read-out-board. The SiPM-signal has a unspecific dip down before the real SiPM-signal starts. A reason could be, that the electronic needs to compensate the saturation of the pixel next to this one (figure 4.16). This figure is created together with N. Höflich [19].

	FACT-fit parameter first measurement				
pixel no.	*gain* [nVs]	crosstalk probability [%]	σ^2_{pe} [$\text{V}^2 \cdot \text{ns}^2$]	σ^2_{el} [$\text{V}^2 \cdot \text{ns}^2$]	χ^2/dof
14	3.128 ± 0.014	0.5115 ± 0.0056	0.215 ± 0.013	0.425 ± 0.024	567/375
15	3.219 ± 0.014	0.4944 ± 0.0060	0.186 ± 0.013	0.498 ± 0.013	605/380
16	3.064 ± 0.018	0.4970 ± 0.0064	0.265 ± 0.015	0.341 ± 0.026	433/332
21	3.128 ± 0.014	0.5213 ± 0.0061	0.184 ± 0.012	0.539 ± 0.023	557/393
22	3.210 ± 0.015	0.4907 ± 0.0062	0.209 ± 0.014	0.474 ± 0.025	594/375
23	3.065 ± 0.015	0.4960 ± 0.0062	0.180 ± 0.013	0.472 ± 0.024	570/369
24	3.148 ± 0.014	0.5030 ± 0.0059	0.209 ± 0.013	0.452 ± 0.024	509/364
29	3.116 ± 0.010	0.5139 ± 0.0056	0.132 ± 0.009	0.552 ± 0.019	502/393
30	3.122 ± 0.013	0.5261 ± 0.0060	0.175 ± 0.011	0.527 ± 0.022	557/382
31	3.128 ± 0.013	0.5173 ± 0.0063	0.166 ± 0.012	0.490 ± 0.023	612/367
32	3.092 ± 0.017	0.5052 ± 0.0064	0.217 ± 0.014	0.462 ± 0.025	551/382
33	3.100 ± 0.014	0.4977 ± 0.0062	0.182 ± 0.012	0.449 ± 0.022	575/391
38	3.188 ± 0.013	0.4734 ± 0.0058	0.167 ± 0.011	0.539 ± 0.021	428/341
39	3.144 ± 0.012	0.5007 ± 0.0061	0.170 ± 0.011	0.454 ± 0.021	522/371
40	3.116 ± 0.012	0.4968 ± 0.0058	0.145 ± 0.010	0.543 ± 0.020	500/381
41	3.146 ± 0.014	0.5109 ± 0.0062	0.187 ± 0.012	0.455 ± 0.023	593/371
46	3.188 ± 0.012	0.4975 ± 0.0060	0.176 ± 0.011	0.490 ± 0.021	519/380
47	3.184 ± 0.012	0.5127 ± 0.0058	0.173 ± 0.011	0.527 ± 0.021	519/377
48	3.142 ± 0.015	0.4886 ± 0.0062	0.179 ± 0.013	0.502 ± 0.024	556/372
63	3.272 ± 0.013	0.5070 ± 0.0062	0.184 ± 0.012	0.473 ± 0.023	656/384

Table 5.1: Parameters of the used SiPMs, calculated with the FACT-fit during the first measurement with the oscilloscope.

	FACT-fit parameter second measurement				
pixel no.	*gain* [nVs]	crosstalk probability [%]	σ^2_{pe} [$\text{V}^2 \cdot \text{ns}^2$]	σ^2_{el} [$\text{V}^2 \cdot \text{ns}^2$]	χ^2/dof
14	3.131 ± 0.014	0.5138 ± 0.0057	0.213 ± 0.014	0.454 ± 0.024	581/384
15	3.145 ± 0.017	0.5050 ± 0.0062	0.185 ± 0.013	0.498 ± 0.024	605/380
16	3.097 ± 0.015	0.4963 ± 0.0059	0.265 ± 0.015	0.341 ± 0.026	433/332
21	3.129 ± 0.014	0.5251 ± 0.0060	0.183 ± 0.012	0.539 ± 0.023	557/393
22	3.204 ± 0.014	0.4875 ± 0.0060	0.200 ± 0.013	0.499 ± 0.025	502/341
23	3.069 ± 0.012	0.4870 ± 0.0058	0.157 ± 0.011	0.488 ± 0.020	533/385
24	3.133 ± 0.014	0.5101 ± 0.0058	0.210 ± 0.013	0.441 ± 0.023	512/374
29	3.142 ± 0.012	0.5037 ± 0.0060	0.140 ± 0.010	0.569 ± 0.021	558/382
30	3.148 ± 0.013	0.5133 ± 0.0058	0.164 ± 0.011	0.561 ± 0.022	548/369
31	3.117 ± 0.012	0.5144 ± 0.0059	0.180 ± 0.011	0.464 ± 0.021	532/381
32	3.077 ± 0.018	0.5129 ± 0.0064	0.237 ± 0.016	0.431 ± 0.027	580/391
33	3.097 ± 0.012	0.5097 ± 0.0057	0.189 ± 0.011	0.438 ± 0.020	449/376
38	3.148 ± 0.013	0.4967 ± 0.0057	0.185 ± 0.011	0.466 ± 0.021	502/388
39	3.165 ± 0.010	0.4936 ± 0.0055	0.154 ± 0.009	0.480 ± 0.019	479/393
40	3.116 ± 0.011	0.4912 ± 0.0056	0.139 ± 0.010	0.560 ± 0.019	507/393
41	3.143 ± 0.013	0.5053 ± 0.0061	0.183 ± 0.012	0.482 ± 0.022	532/373
46	3.174 ± 0.014	0.5024 ± 0.0062	0.190 ± 0.012	0.451 ± 0.023	601/384
47	3.157 ± 0.013	0.5227 ± 0.0063	0.175 ± 0.012	0.501 ± 0.023	621/377
48	3.154 ± 0.015	0.4956 ± 0.0064	0.190 ± 0.013	0.475 ± 0.024	571/363
63	3.273 ± 0.013	0.5115 ± 0.0063	0.192 ± 0.012	0.467 ± 0.023	591/368

Table 5.2: Parameters of the used SiPMs, calculated with the FACT-fit during the first measurement with the oscilloscope.

Erklärung

Hiermit versichere ich, dass ich diese Arbeit einschließlich beigefügter Zeichnungen, Darstellungen und Tabellen selbstständig angefertigt und keine anderen als die angegebenen Hilfsmittel und Quellen benutzt habe. Alle Stellen, die dem Wortlaut oder dem Sinn nach anderen Werken entnommen sind, habe ich in jedem einzelnen Fall unter genauer Angabe der Quelle deutlich als Entlehnung kenntlich gemacht.

Aachen, den September 27, 2016

_____

Benjamin Jan Pestka